

# The Sky Distribution and Magnitudes of Starlink Satellites by the Year 2027

Anthony Mallama

anthony.mallama@gmail.com

2022 September 1

## Abstract

Visual magnitudes and sky coordinates are projected for the full constellation of Starlink satellites. The results are presented in the form of sky maps and numerical tables. Observer latitudes from the equator to  $60^\circ$  are considered. The solar elevations include  $-12^\circ$  (the end of nautical twilight),  $-18^\circ$  (the end of astronomical twilight) and  $-30^\circ$ .

## 1. Introduction

The largest group of spacecraft currently in orbit is the constellation of Starlink satellites. They presently number over 2,000 and are projected to total nearly 12,000 by year 2027. Professional astronomers are already experiencing interference from Starlink spacecraft when making celestial observations (Mroz et al., 2022) and amateur stargazers are concerned as well for both scientific and aesthetic reasons (Mallama and Young, 2021). The International Astronomical Union has established a Centre for the Protection of Dark and Quiet Skies from Satellite Constellation Interference to address this problem. A reading list of papers on satellite constellations and their impact is provided in Appendix A.

This paper forecasts the distribution and brightness of Starlink satellites in the sky after the entire constellation is in place. The method is to compute the azimuth, elevation and range for each satellite visible at ground locations from the equator to latitude  $60^\circ$ . These coordinates are based on spacecraft orbital elements and they allow for computation of the apparent magnitude. Brightness is calculated from a phase curve equation derived from visual magnitudes.

Section 2 lists the spacecraft orbital elements and describes the method of computing satellite topocentric coordinates. The method of determining whether a satellite is in sunlight or in the Earth's shadow is also explained. Section 3 describes the phase functions for three Starlink satellite designs. These curves characterize brightness versus the phase angle which is measured at the satellite between the Sun and the Earth. Then the equation for computing apparent magnitudes is presented. More details about the Starlink phase functions can be found in Appendix B. Section 4 gives examples of resulting sky maps which plot satellite locations by azimuth, elevation and magnitude. Sample tables of numerical results are also provided. Comprehensive sets of map and numerical results for a wide range of observer latitude and solar distances below the horizon are given in Appendix C. Section 5 considers the limitations and uncertainties in this study. Section 6 presents the conclusions and compares the satellite number density to an earlier forecast made by McDowell (2020).

## 2. Satellite orbits and celestial coordinates

Starlink satellites will occupy in 8 'shells' at altitudes ranging from 336 to 570 km as listed in Table 1. There are several orbital planes for each shell and a number of satellites in each plane. For this study the ascending nodes of the planes for each shell are distributed evenly over  $2\pi$  radians. Likewise, the orbital

anomaly for each satellite in a plane is  $2\pi$  divided by the number of satellites in that plane. The geocentric coordinates of satellites are determined from the elements including the anomalies. Examples of these coordinates for the satellites in medium inclination and high inclination shells are shown in Figures 1 and 2, respectively.

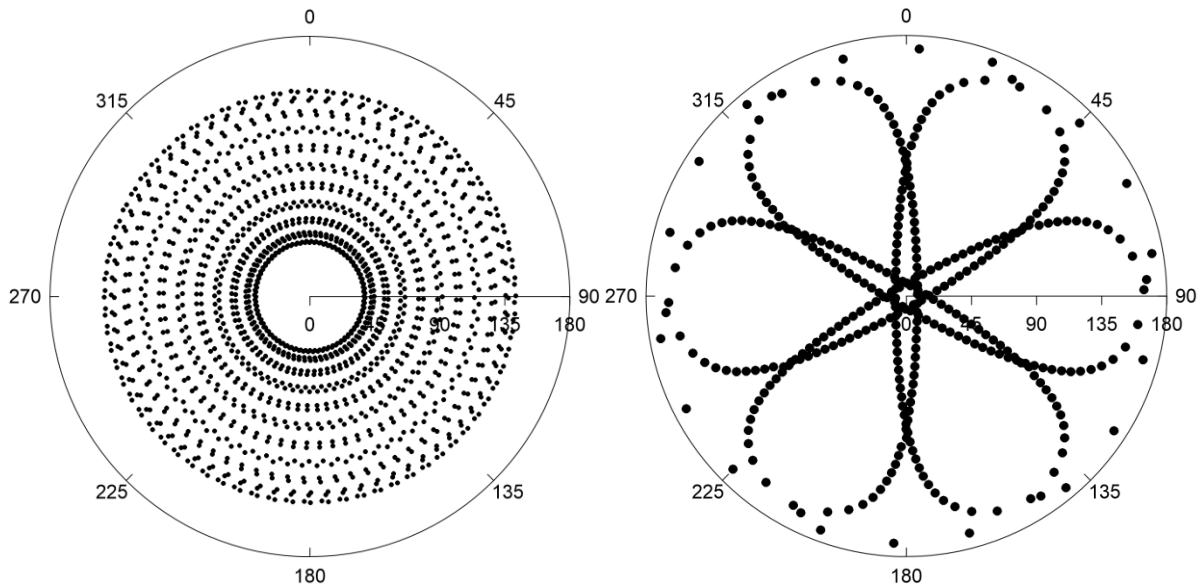


Figure 1 (left). The distribution of satellites in shell 1 with orbital inclination 53.0 degrees is shown as a polar plot with the radial axis extending from 0 degrees in the direction of the north pole of the Earth's axis to 180 in the opposite direction. Satellite positions are concentrated toward the equator and away from the poles.

Figure 2 (right). The distribution of satellites in shell 4 with orbital inclination 97.6 degrees is illustrated. Satellite positions are more concentrated toward polar latitudes than in Figure 1.

Table 1. Orbital information

Shell	1	2	3	4	5	6	7	8
Altitudes	550.	540.	570.	560.	560.	336.	341.	346.
Inclinations	53.0	53.2	70.0	97.6	97.6	42.0	48.0	53.0
Planes	72	72	36	6	4	50	50	50
Sats_per_plane	22	22	20	58	43	50	50	50

The information in Table 1 is taken from [https://en.wikipedia.org/wiki/Starlink\\_as\\_retrieved\\_on\\_2022\\_July\\_15](https://en.wikipedia.org/wiki/Starlink_as_retrieved_on_2022_July_15). 'Planes' here is 'count' in the source document, and 'sats\_per\_plane' here is 'sat\_per' in the source. The number of planes and satellites per plane for shells 6 through 8 was not listed in the source document, so each is taken to be approximately the square root of 'satellites' there.

The satellite azimuth and elevation at a selected ground location are determined by transforming its geocentric coordinates to topocentric values at the latitude and longitude on the ground. Examples of the satellite azimuths and elevations shown in Figures 3 and 4 illustrate how the distribution changes with observer latitude.

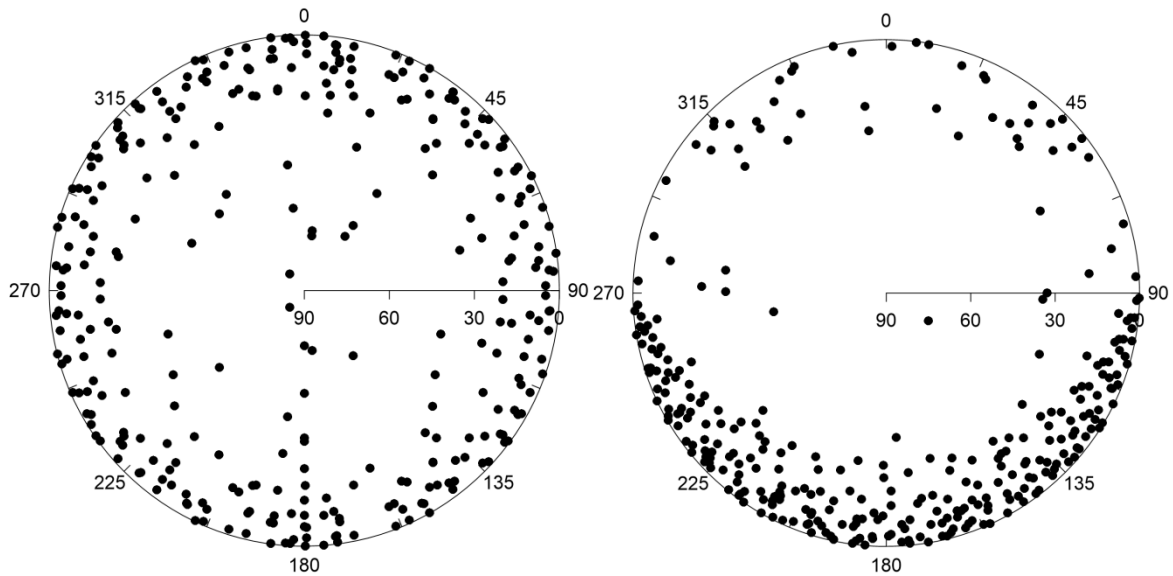


Figure 3 (left). The distribution of satellites above the horizon as seen from the equator is plotted. Density increases with distance from zenith but the azimuthal distribution is practically uniform.

Figure 4 (right). The satellite distribution as seen from latitude 60° north is heavily concentrated toward the south (azimuth 180) because most orbital inclinations are less than that latitude.

Satellites may be hidden from sunlight by the Earth's shadow in which case they do not interfere with optical astronomy. The shadow limit at a shell's orbital altitude corresponds to an angular radius measured at center of the Earth relative to a line extending from the Sun through that geocenter location. The radius values are given by the arc-cosine of the Earth's radius divided by the distance of a satellite from the geocenter. These shadow radii range from about 67° for the highest altitude satellites to 72° for the lowest. Figures 7 and 8 in Section 4 illustrate how the Earth's shadow eclipses satellites over a larger area of sky as the Sun's distance below the horizon grows.

### 3. Phase function and satellite brightness

Phase curves describe spacecraft brightness as a function of the angle measured at the satellite between the Sun and the observer. The chassis of a Starlink spacecraft is shaped like a flat panel and its

orientation is nominally perpendicular to the nadir-zenith direction. Additionally, there is a large solar array attached at a right angle to the zenith-facing side of the panel and it projects upward. These components are shown schematically in Figure 5 along with their orientation in space.

Sunlight scatters from Starlink spacecraft in a manner that differs sharply from that of round bodies like the Moon and planets. Those celestial bodies preferentially reflect light back in the direction from which it originated. Starlink spacecraft, on the other hand, reflect sunlight both backwards and forwards. The forward scattering is likely due to a near-specular reflection from the flat nadir side.

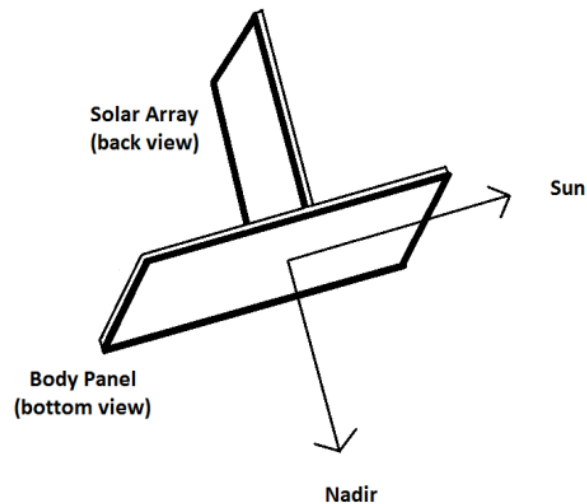


Figure 5. This schematic of the Starlink spacecraft illustrates its shape and orientation relative to the Sun and Earth.

There have been two changes to the detailed design of Starlink satellites, so far. The Original Design was the brightest and about 400 spacecraft (<https://planet4589.org/space/stats/star/starstats.html>, derived from data retrieved 2022 June 15) were launched before it was modified in response to the concerns of astronomers. The manufacturer, SpaceX, added a sunshade to help reduce luminosity and about 1,100 of this new model, called VisorSat, were launched (ibid). VisorSats were typically 1.3 magnitudes fainter than the Original Design (Mallama, 2021a) at operational altitudes. However, when SpaceX upgraded the communication system for Starlink from radio to laser in 2021 the sunshades had to be dropped from the design (Witze, 2022). In order to compensate for removing the shades SpaceX began development of reflective materials for the nadir side of the flat panel to direct sunlight away from observers beneath the spacecraft. The new design occurred at about serial number 3000 and so this latest model is referred to as Series-3000 herein. This latest design of Starlink is typically about 0.5 magnitudes brighter than VisorSats although it is still approximately 0.8 magnitudes fainter than the Original Design (Mallama, 2022).

Besides their different characteristic luminosities each Starlink design has its own distinct phase function. Figure 6 shows that the response for the Original Design is relatively flat, while that of VisorSat

is strongly curved and that for Series-3000 is intermediate between the two. Since the phase function for Series-3000 lies between the two others and because this model represents the current Starlink design, the magnitudes in this paper rely on its phase function as indicated by Eq. 1,

$$v = 3.817 + 0.06970 \phi - 0.0003999 \phi^2 + 5 \log (d / 1000)$$

Eq. 1

where  $v$  is the apparent visual magnitude,  $\phi$  is the phase angle in degrees, and  $d$  is the distance from the satellite to the observer in km. The distance term accounts for the inverse square law of light.

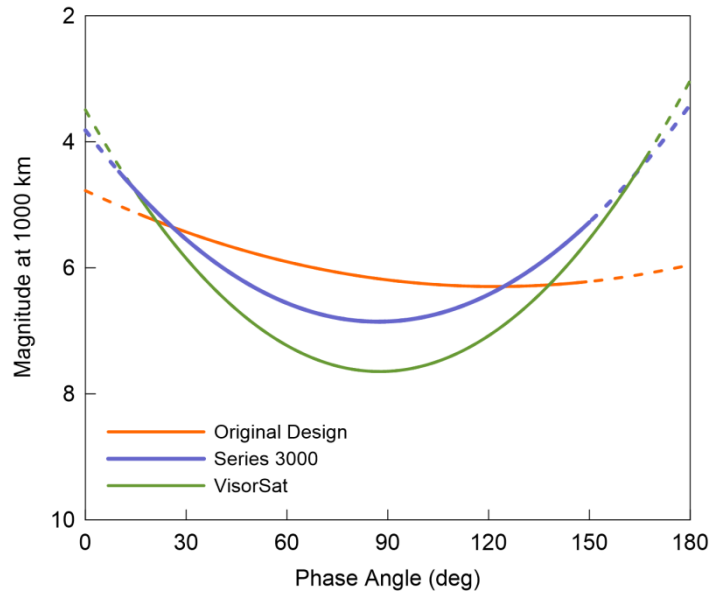


Figure 6. Phase functions corresponding to the three Starlink designs for spacecraft at their operational altitudes. The visual magnitudes used to derive these functions are close to the V-band of the Johnson-Cousins photometric system of electronic measurements. Dashed lines are extrapolations beyond the observed range; satellites are rarely seen at these extreme phase angles.

The phase function accounts for some of the apparent brightness of Starlink satellites. However, their complex shapes make the luminosity sensitive to spacecraft attitude (yaw, pitch and roll) in a way that is not yet generally understood. Brightness variations due to attitude appear as scatter in an empirically derived phase function diagram. A study of Starlink magnitudes (Mallama, 2021b) indicated that this scatter was about 0.4 magnitudes after observational uncertainties were removed. Therefore, the apparent magnitudes computed in this paper have that amount of scatter applied. The Box-Muller algorithm for normal statistical distributions as implemented here:

[https://masuday.github.io/fortran\\_tutorial/random.html](https://masuday.github.io/fortran_tutorial/random.html) is employed. More details about the Starlink phase function and the scatter are provided in Appendix B.

#### 4. Distribution in the sky and apparent magnitudes

The geometric and photometric aspects of Starlink satellites discussed in the previous two sections allow for simulation of their appearance in the sky. Examples of sky maps showing distributions and magnitudes as well as numerical output are presented in this section. The statistical results include satellite counts by magnitude, by elevation and by quadrant of the sky, as well as the number of satellites in sunlight and in shadow.

Maps for an observer at the terrestrial equator and with the Sun on the celestial equator are shown as Figures 7 and 8, while corresponding numerical data is given in Tables 2 and 3. At the end of astronomical twilight when the Sun is  $18^\circ$  below the horizon (Figure 7 and Table 2) satellites are visible in all quadrants of the sky; 89 of them are brighter than magnitude 7, and 21 of those are above  $30^\circ$  elevation. When the Sun has descended to  $30^\circ$  below the horizon (Figure 8 and Table 3) there no satellites visible in the quadrants opposite the solar azimuth; only 19 satellites are brighter than magnitude 7 and none of those are above  $30^\circ$  elevation.

Similar maps and tables for observer latitudes from the equator to  $60^\circ$  are presented in Appendix C. Results are given for the dates of solstice and equinox, and for solar distances of  $12^\circ$ ,  $18^\circ$  and  $30^\circ$  below the horizon. The distribution and magnitudes of satellites is discussed in the Section 6.

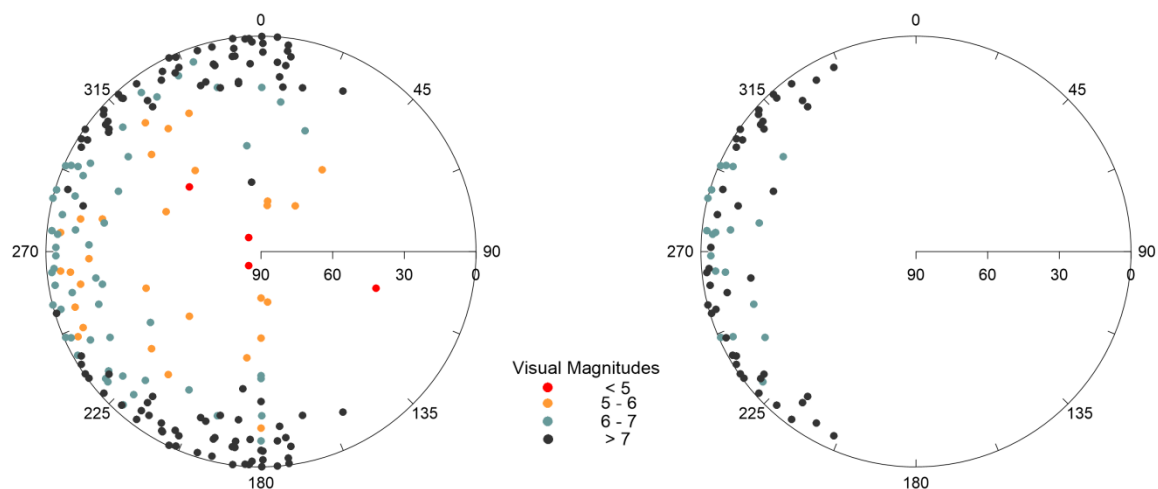


Figure 7 (left). The distribution and brightness of Starlink satellites for an observer at the equator on a date of equinox with the Sun  $18^\circ$  below the horizon at azimuth  $270^\circ$  is plotted.

Figure 8 (right). The Sun is  $30^\circ$  below azimuth  $270^\circ$ . This plot along with Figure 7 illustrates how the Earth's shadow progressively hides more satellites as the Sun descends further below the horizon. They also demonstrate how the forward-scattering phase curve enhances the brightness of satellites that are aligned with the solar azimuth.

Table 2. Satellite locations and magnitudes corresponding to Figure 7.

Latitude	0.0, solar az. 270.0,		solar el. -18.0,		solar dec. 0.0		----- Quadrant -----				
Magni- tude	Northwest		Southwest		Southeast		Northeast		All Quadrants		
	30+	30-	30+	30-	30+	30-	30+	30-	30+	30-	Any
< 5	2	0	1	0	1	0	0	0	4	0	4
5 - 6	2	7	3	9	3	1	4	0	12	17	29
6 - 7	1	23	1	24	2	2	1	2	5	51	56
> 7	1	41	1	36	0	15	0	13	2	105	107
Sunlit	6	71	6	69	6	18	5	15	23	173	196
Shadow	0	0	0	0	2	56	2	59	4	115	119
All	6	71	6	69	8	74	7	74	27	288	315

Table 3. Satellite locations and magnitudes corresponding to Figure 8.

Latitude	0.0, solar az. 270.0,		solar el. -30.0,		solar dec. 0.0		----- Quadrant -----				
Magni- tude	Northwest		Southwest		Southeast		Northeast		All Quadrants		
	30+	30-	30+	30-	30+	30-	30+	30-	30+	30-	Any
< 5	0	0	0	0	0	0	0	0	0	0	0
5 - 6	0	0	0	0	0	0	0	0	0	0	0
6 - 7	0	11	0	8	0	0	0	0	0	19	19
> 7	0	21	0	23	0	0	0	0	0	44	44
Sunlit	0	32	0	31	0	0	0	0	0	63	63
Shadow	6	39	6	38	8	74	7	74	27	225	252
All	6	71	6	69	8	74	7	74	27	288	315

### 5. Limitations of this study

Several factors place limits on the results presented here. Most importantly, the future of the Starlink constellation is uncertain. The source of the orbital data listed in Table 1 does not give complete Keplerian elements and some assumptions had to be made as stated there. Furthermore, since only a fraction of the satellites have actually been launched the actual configuration and number of the Starlink satellites in space may turn out to be different. Also, the projected completion date for launching all of the nearly 12,000 satellites may not be met.

Another issue is the phase curve. The magnitudes in this study are computed from the curve for Series-3000 satellites. However, there have already been three Starlink designs and each has had its own distinctive reflection characteristics and phase curve. Future design modifications would likely result in new phase functions.

Besides changes to the shape of Starlink satellites, SpaceX CEO Elon Musk has stated in this video [https://youtu.be/XP5k3ZzPf\\_0?t=561](https://youtu.be/XP5k3ZzPf_0?t=561) that the future Starlink 2.0 will be a larger spacecraft with a length of 7 meters. This increased size may reflect more light and appear brighter in the sky.



Finally, SpaceX has requested approval to launch 30,000 satellites in addition to the 12,000 already approved. So, the sky could become much more crowded with bright satellites than this study projects.

## 6. Conclusions

The sky maps and numerical results in Section 4 and in Appendix C indicate the impact of Starlink satellites on celestial observation by the year 2027. During astronomical twilight hundreds of spacecraft brighter than magnitude 7 will be visible from any one location. However, most of those will be within  $30^\circ$  of the horizon and only tens of satellites will be seen at higher elevations. The number of visible satellite diminishes rapidly after astronomical twilight ends.

Additionally, spacecraft that are aligned with the solar azimuth and those opposite that azimuth tend to be brighter because of forward and backward scattering of light. Finally, the density of satellites is greater toward celestial south for an observer north of the terrestrial equator and vice-versa due to the geocentric distribution of satellites.

Finally, the results obtained here are compared with two previous studies. First, McDowell (2020) forecast “a latitude-dependent areal number density of between 0.005 and 0.01 objects per square degree at airmass  $<2$ ”. The corresponding numbers from this study range from 0.003 at the equator to 0.006 at  $50^\circ$  latitude. These smaller densities are due lower orbital altitudes for satellites in shells 2 through 5. At the time of McDowell’s study these heights were expected to range from 1110 to 1325 km but now they are from 540 to 560. Second, Lawler et al. (2022) predict that latitudes near  $50^\circ$  will experience the worst satellite interference. This analysis finds that the number density increases to that latitude as noted above, and then it falls off sharply by latitude  $60^\circ$ . So, these findings agree.

### Appendix A. Reading list of papers on satellite constellation interference

These papers are grouped by subject matter as follows: impacts on observations, working group reports and conference material, satellite brightness, mitigation strategies and general. Titles are given here to indicate content while full citations are provided in the Reference section.

#### Appendix A-1. Impacts on celestial observations

Gallozzi et al. 2020. Concerns about ground based astronomical observations: a step to safeguard the astronomical sky.

Hainaut and Williams, 2020. Impact of satellite constellations on astronomical observations with ESO telescopes in the visible and infrared domains.

McDowell, 2020. The low Earth orbit satellite population and impacts of the SpaceX Starlink constellation.

Mroz et al. 2022. Impact of the SpaceX Starlink satellites on the Zwicky Transient Facility survey observations.

Williams et al. 2021b. A report to ESO Council on the impact of satellite constellations.

Walker et al. 2020a. Impact of satellite constellations on optical astronomy and recommendations toward mitigations.

Williams et al. 2021a. Analysing the impact of satellite constellations and ESO's role in supporting the astronomy community.

#### Appendix A-2. Working group reports and conference proceedings

Hall et al. 2021. SatCon2 Working Group Reports.

Walker and Benvenuti, 2022. Dark and Quiet Skies for Science and Society II.

Walker et al. 2020b. Dark and quiet skies for science and society.

Otarola et al. 2020. Draft Report of the Satellite Observations Working Group.

#### Appendix A-3. Satellite brightness

Halferty et al. 2022. Photometric characterization and trajectory accuracy of Starlink satellites: implications for ground-based astronomical surveys.

Hosseini et al. 2022. Photometric characterization of Starlink satellite tracklets using RGB filters.

Krantz et al. 2021. Characterizing the all-sky brightness of satellite mega-constellations and the impact on astronomy research.

Mallama, 2021a. The brightness of VisorSat-design Starlink satellites.

Mallama, 2021b. Starlink satellite brightness – characterized from 100,000 visible light magnitudes.

Mallama, 2022. Newest Starlink satellites have gotten brighter again.

Tregloan-Reed et al. 2020. First observations and magnitude measurement of Starlink's Darksat.

#### Appendix A-4. Mitigation strategies

Tyson et al. 2020. Mitigation of LEO satellite brightness and trail effects on the Rubin Observatory LSST.

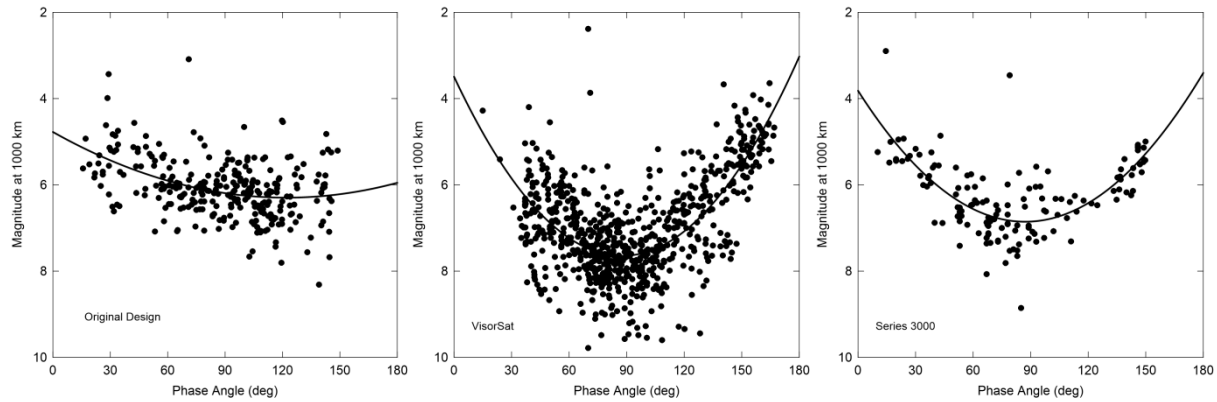
#### Appendix A-5. General audience

Mallama and Young, 2021. The satellite saga continues.

Witze, 2022. 'Unsustainable': how satellite swarms pose a rising threat to astronomy.

#### Appendix B. Phase functions

The material in this appendix supplements the discussion of phase functions in Section 3. The empirically derived phase functions for Original Design, VisorSat and Series-3000 spacecraft plotted in Figure X are shown along with the observations in Figures B-1, B-2 and B-3.



Figures B-1, B-2 and B-3 (left to right). The observed and modeled phase curves for Original Design, VisorSat and Series-3000 Starlink satellites are compared. The scatter is mostly due to variations in spacecraft attitude (yaw, pitch and roll).

A study of Starlink magnitudes measured electronically (Mallama 2021b) revealed that phase functions can change with time as illustrated in Figure B-4. This variation may have resulted from systematic changes to spacecraft attitude.

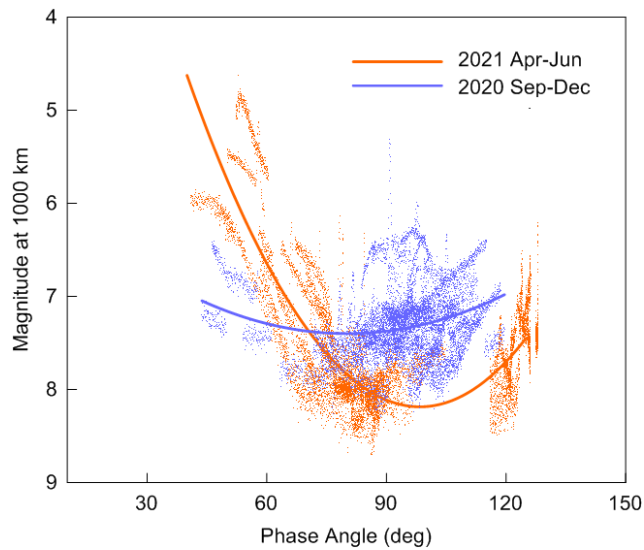
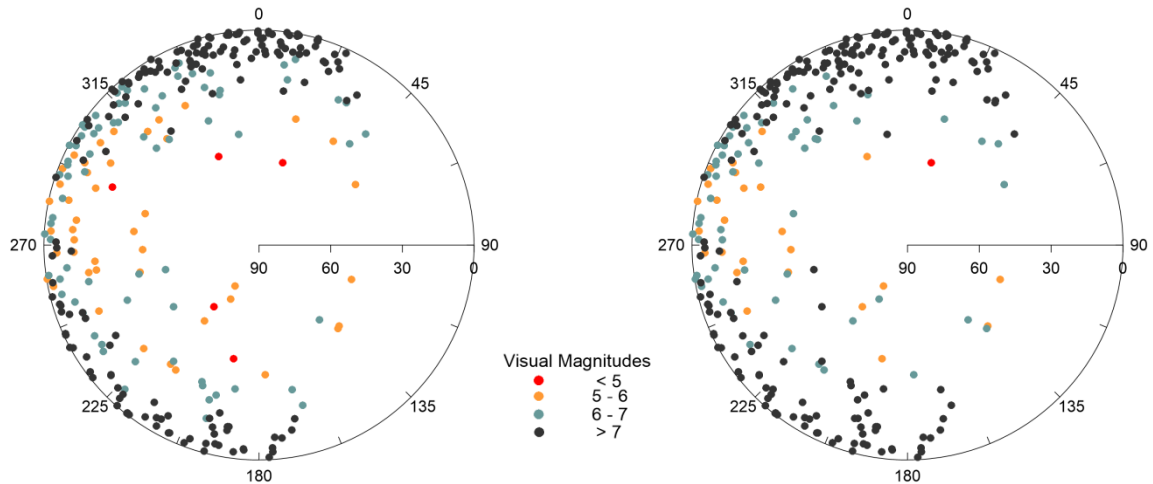


Figure B-4. Two markedly different VisorSat phase functions separated by several months are illustrated.

The plots in Figures B-5 and B-6 demonstrate moderate sensitivity of magnitudes in the sky to phase function by comparing Series-3000 to VisorSat. The magnitudes for Series-3000 are somewhat brighter at high elevations. This result is consistent with the phase curves in B-2 and B-3 where VisorSats are fainter around phase angle  $90^\circ$ . At low elevations the magnitudes are more nearly equal.



Figures B-5 (left) and B-6 are for an observer at  $30^\circ$  latitude with the Sun  $18^\circ$  below the horizon at azimuth  $281^\circ$ . B-5 is for the Series-3000 phase function and B-6 is for VisorSat.

The phase curves were derived from visual magnitudes observed by Jay Respler at latitude  $40.330$  and longitude  $74.445$  west, and by the author at  $38.982$  and  $76.763$ . They are reported at <http://www.satobs.org/seesat/index.html>.

### Appendix C. Sky maps and numerical tables for latitudes from $10^\circ$ to $60^\circ$

Results for observer latitudes  $0^\circ$  through  $60^\circ$  are presented in appendix sections C-0 through C-6. Each section is divided into subsections  $\alpha$ ,  $\beta$  and  $\gamma$  for the Sun at declinations  $-23.4^\circ$  (winter solstice),  $0.0^\circ$  (equinox) and  $+23.4^\circ$  (summer solstice). The subsections contain sky maps and numerical results for the Sun's distance below the horizon of  $12^\circ$  (end of nautical twilight),  $18^\circ$  (end of astronomical twilight) and  $30^\circ$ , respectively. For example, in Appendix C-0- $\alpha$  the number '0' is for latitude  $0^\circ$ , the ' $\alpha$ ' is for solar declination  $-23.4^\circ$ , and the results include solar zenith angles of  $102^\circ$ ,  $108^\circ$  and  $120^\circ$ . The maps and numerical results for southern observer latitudes are the same as their northern counterparts with two trivial exceptions; the sky quadrants on each side of the east-west line are reversed and the solar declinations are switched on the solstice dates.

Appendix C-0- $\alpha$ . Latitude  $0^\circ$ , solar declination  $-23.4^\circ$

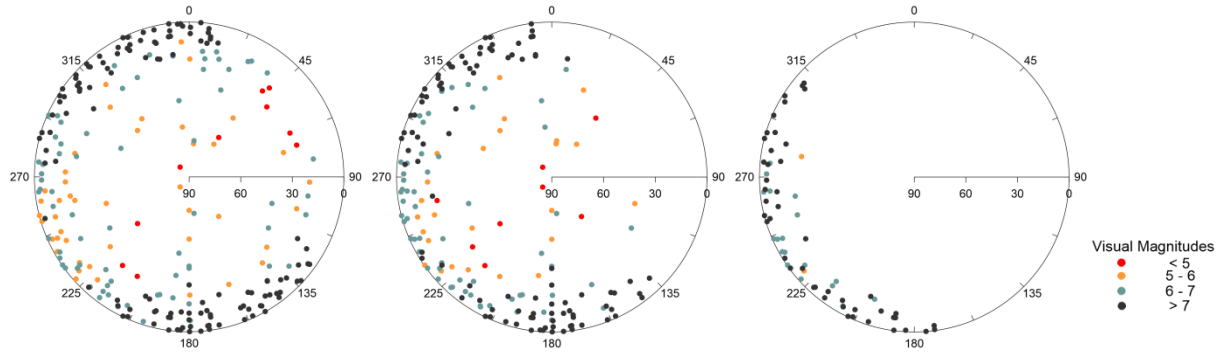


Figure C-0- $\alpha$ . The distribution and brightness of Starlink satellites is illustrated for an observer at the equator on a date when the Sun is at declination  $-23.4^\circ$ . From left to right the Sun's distance below the western horizon is  $12^\circ$  (end of nautical twilight),  $18^\circ$  (end of astronomical twilight) and  $30^\circ$ .

Table C-0- $\alpha$ . Latitude  $0^\circ$ , solar declination  $-23.4^\circ$

Latitude 0.0, solar az. 246.0, solar el. -12.0, solar dec. -23.4											
----- Quadrant -----											
Magni- tude	Northwest		Southwest		Southeast		Northeast		All Quadrants		
	30+	30-	30+	30-	30+	30-	30+	30-	30+	30-	Any
< 5	1	0	1	2	0	0	1	5	3	7	10
5 - 6	3	5	2	20	3	6	4	1	12	32	44
6 - 7	2	16	3	27	5	6	2	10	12	59	71
> 7	0	50	0	20	0	43	0	10	0	123	123
Sunlit	6	71	6	69	8	55	7	26	27	221	248
Shadow	0	0	0	0	0	19	0	48	0	67	67
All	6	71	6	69	8	74	7	74	27	288	315

Latitude 0.0, solar az. 245.3, solar el. -18.0, solar dec. -23.4											
----- Quadrant -----											
Magni- tude	Northwest		Southwest		Southeast		Northeast		All Quadrants		
	30+	30-	30+	30-	30+	30-	30+	30-	30+	30-	Any
< 5	1	0	2	3	1	0	1	0	5	3	8
5 - 6	3	2	2	11	3	0	4	0	12	13	25
6 - 7	2	14	2	33	3	4	0	1	7	52	59
> 7	0	46	0	22	1	28	0	1	1	97	98
Sunlit	6	62	6	69	8	32	5	2	25	165	190
Shadow	0	9	0	0	0	42	2	72	2	123	125
All	6	71	6	69	8	74	7	74	27	288	315

Latitude 0.0, solar az. 242.7, solar el. -30.0, solar dec. -23.4											
----- Quadrant -----											
Magni- tude	Northwest		Southwest		Southeast		Northeast		All Quadrants		
	30+	30-	30+	30-	30+	30-	30+	30-	30+	30-	Any
< 5	0	0	0	0	0	0	0	0	0	0	0
5 - 6	0	1	0	1	0	0	0	0	0	2	2
6 - 7	0	2	0	16	0	0	0	0	0	18	18
> 7	0	14	0	29	0	3	0	0	0	46	46
Sunlit	0	17	0	46	0	3	0	0	0	66	66
Shadow	6	54	6	23	8	71	7	74	27	222	249
All	6	71	6	69	8	74	7	74	27	288	315

Appendix C-0-β. Latitude 0°, solar declination 0.0°

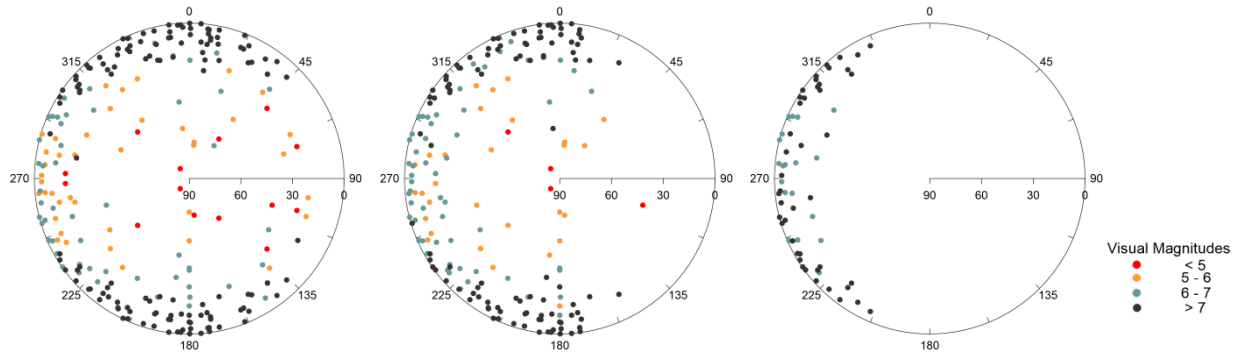


Figure C-0-β. The distribution and brightness of Starlink satellites is illustrated for an observer at the equator on a date when the Sun is at declination 0.0°. From left to right the Sun’s distance below the western horizon is 12° (end of nautical twilight), 18° (end of astronomical twilight) and 30°.

Table C-0-β. Latitude 0°, solar declination 0.0°

Latitude	0.0,		solar az. 270.0,		solar el. -12.0,		solar dec. 0.0		-----		
	Quadrant										
Magni-	Northwest		Southwest		Southeast		Northeast		All Quadrants		
tude	30+	30-	30+	30-	30+	30-	30+	30-	30+	30-	Any
< 5	2	1	2	1	3	2	1	2	8	6	14
5 - 6	3	12	1	13	2	3	4	3	10	31	41
6 - 7	1	15	3	19	3	7	2	4	9	45	54
> 7	0	43	0	36	0	27	0	28	0	134	134
Sunlit	6	71	6	69	8	39	7	37	27	216	243
Shadow	0	0	0	0	0	35	0	37	0	72	72
All	6	71	6	69	8	74	7	74	27	288	315

Latitude	0.0,		solar az. 270.0,		solar el. -18.0,		solar dec. 0.0		-----		
	Quadrant										
Magni-	Northwest		Southwest		Southeast		Northeast		All Quadrants		
tude	30+	30-	30+	30-	30+	30-	30+	30-	30+	30-	Any
< 5	2	0	1	0	1	0	0	0	4	0	4
5 - 6	2	7	3	9	3	1	4	0	12	17	29
6 - 7	1	23	1	24	2	2	1	2	5	51	56
> 7	1	41	1	36	0	15	0	13	2	105	107
Sunlit	6	71	6	69	6	18	5	15	23	173	196
Shadow	0	0	0	0	2	56	2	59	4	115	119
All	6	71	6	69	8	74	7	74	27	288	315

Latitude	0.0,		solar az. 270.0,		solar el. -30.0,		solar dec. 0.0		-----		
	Quadrant										
Magni-	Northwest		Southwest		Southeast		Northeast		All Quadrants		
tude	30+	30-	30+	30-	30+	30-	30+	30-	30+	30-	Any
< 5	0	0	0	0	0	0	0	0	0	0	0
5 - 6	0	0	0	0	0	0	0	0	0	0	0
6 - 7	0	11	0	8	0	0	0	0	0	19	19
> 7	0	21	0	23	0	0	0	0	0	44	44
Sunlit	0	32	0	31	0	0	0	0	0	63	63
Shadow	6	39	6	38	8	74	7	74	27	225	252
All	6	71	6	69	8	74	7	74	27	288	315

Appendix C-0-γ. Latitude 0°, solar declination +23.4°

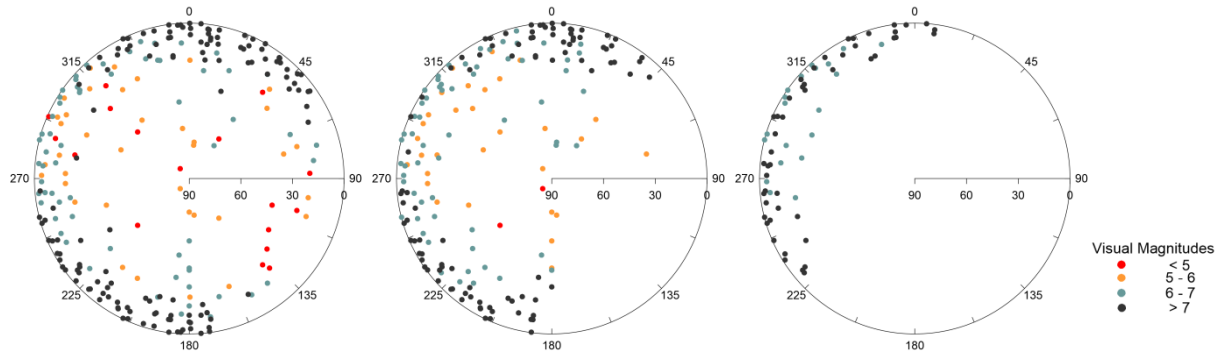


Figure C-0-γ. The distribution and brightness of Starlink satellites is illustrated for an observer at the equator on a date when the Sun is at declination +23.4°. From left to right the Sun's distance below the western horizon is 12° (end of nautical twilight), 18° (end of astronomical twilight) and 30°.

Table C-0-γ. Latitude 0°, solar declination +23.4°

Latitude	0.0, solar az. 294.0, solar el. -12.0, solar dec. 23.4										
	----- Quadrant -----										
Magni-	Northwest		Southwest		Southeast		Northeast		All Quadrants		
tude	30+	30-	30+	30-	30+	30-	30+	30-	30+	30-	Any
< 5	2	5	1	0	2	4	1	2	6	11	17
5 - 6	3	14	2	4	3	4	3	4	11	26	37
6 - 7	1	27	2	15	3	6	2	7	8	55	63
> 7	0	25	1	50	0	13	1	43	2	131	133
Sunlit	6	71	6	69	8	27	7	56	27	223	250
Shadow	0	0	0	0	0	47	0	18	0	65	65
All	6	71	6	69	8	74	7	74	27	288	315

Latitude	0.0, solar az. 294.7, solar el. -18.0, solar dec. 23.4										
	----- Quadrant -----										
Magni-	Northwest		Southwest		Southeast		Northeast		All Quadrants		
tude	30+	30-	30+	30-	30+	30-	30+	30-	30+	30-	Any
< 5	0	0	2	0	0	0	0	0	2	0	2
5 - 6	4	16	1	2	4	0	3	0	12	18	30
6 - 7	2	33	2	16	1	0	4	4	9	53	62
> 7	0	22	1	43	0	1	0	28	1	94	95
Sunlit	6	71	6	61	5	1	7	32	24	165	189
Shadow	0	0	0	8	3	73	0	42	3	123	126
All	6	71	6	69	8	74	7	74	27	288	315

Latitude	0.0, solar az. 297.3, solar el. -30.0, solar dec. 23.4										
	----- Quadrant -----										
Magni-	Northwest		Southwest		Southeast		Northeast		All Quadrants		
tude	30+	30-	30+	30-	30+	30-	30+	30-	30+	30-	Any
< 5	0	0	0	0	0	0	0	0	0	0	0
5 - 6	0	0	0	0	0	0	0	0	0	0	0
6 - 7	0	17	0	3	0	0	0	0	0	20	20
> 7	0	29	0	16	0	0	0	3	0	48	48
Sunlit	0	46	0	19	0	0	0	3	0	68	68
Shadow	6	25	6	50	8	74	7	71	27	220	247
All	6	71	6	69	8	74	7	74	27	288	315

Appendix C-1- $\alpha$ . Latitude  $10^\circ$ , solar declination  $-23.4^\circ$

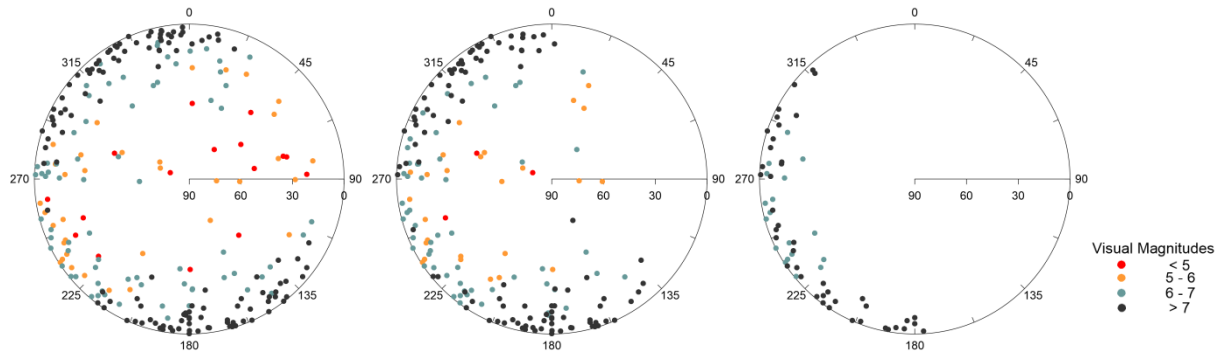


Figure C-1- $\alpha$ . The distribution and brightness of Starlink satellites is illustrated for an observer at latitude  $+10^\circ$  at the winter solstice. From left to right the Sun's distance below the western horizon is  $12^\circ$  (end of nautical twilight),  $18^\circ$  (end of astronomical twilight) and  $30^\circ$ .

Table C-1- $\alpha$ . Latitude  $10^\circ$ , solar declination  $-23.4^\circ$

Latitude 10.0, solar az. 248.0, solar el. -12.0, solar dec. -23.4											
-----											
Quadrant											
Magnitude	Northwest		Southwest		Southeast		Northeast		All Quadrants		
	30+	30-	30+	30-	30+	30-	30+	30-	30+	30-	Any
< 5	2	0	0	4	2	0	7	1	11	5	16
5 - 6	3	6	1	13	3	2	1	6	8	27	35
6 - 7	4	20	2	25	1	11	3	5	10	61	71
> 7	0	54	0	23	0	40	0	7	0	124	124
Sunlit	9	80	3	65	6	53	11	19	29	217	246
Shadow	0	0	0	0	0	18	0	61	0	79	79
All	9	80	3	65	6	71	11	80	29	296	325

Latitude 10.0, solar az. 248.5, solar el. -18.0, solar dec. -23.4											
-----											
Quadrant											
Magnitude	Northwest		Southwest		Southeast		Northeast		All Quadrants		
	30+	30-	30+	30-	30+	30-	30+	30-	30+	30-	Any
< 5	2	0	0	1	0	0	0	0	2	1	3
5 - 6	3	5	2	10	3	0	3	0	11	15	26
6 - 7	4	14	1	30	1	4	1	1	7	49	56
> 7	0	48	0	24	1	29	0	1	1	102	103
Sunlit	9	67	3	65	5	33	4	2	21	167	188
Shadow	0	13	0	0	1	38	7	78	8	129	137
All	9	80	3	65	6	71	11	80	29	296	325

Latitude 10.0, solar az. 248.7, solar el. -30.0, solar dec. -23.4											
-----											
Quadrant											
Magnitude	Northwest		Southwest		Southeast		Northeast		All Quadrants		
	30+	30-	30+	30-	30+	30-	30+	30-	30+	30-	Any
< 5	0	0	0	0	0	0	0	0	0	0	0
5 - 6	0	0	0	0	0	0	0	0	0	0	0
6 - 7	0	5	0	13	0	0	0	0	0	18	18
> 7	0	15	0	25	0	3	0	0	0	43	43
Sunlit	0	20	0	38	0	3	0	0	0	61	61
Shadow	9	60	3	27	6	68	11	80	29	235	264
All	9	80	3	65	6	71	11	80	29	296	325



Appendix C-1-β. Latitude 10°, solar declination 0.0°

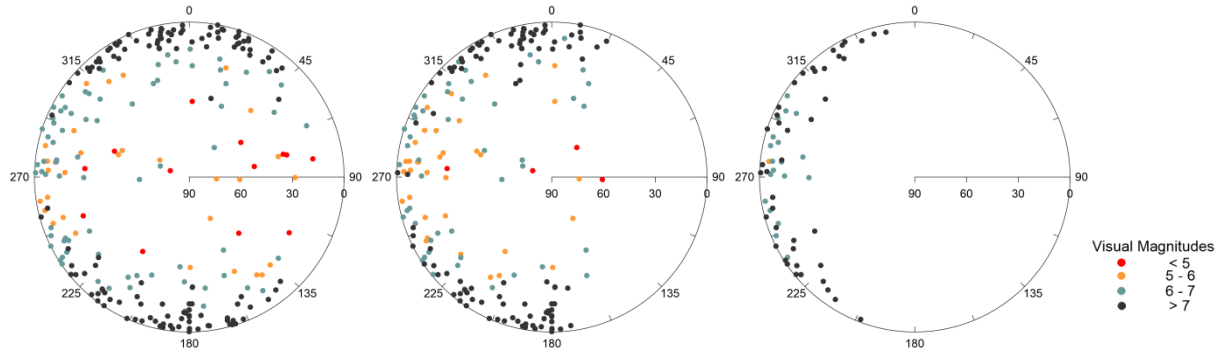


Figure C-1-β. The distribution and brightness of Starlink satellites is illustrated for an observer at latitude +10° at an equinox date. From left to right the Sun's distance below the western horizon is 12° (end of nautical twilight), 18° (end of astronomical twilight) and 30°.

Table C-1-β. Latitude 10°, solar declination 0.0°

Latitude 10.0, solar az. 272.1, solar el. -12.0, solar dec. 0.0

Magnitude	Northwest		Southwest		Southeast		Northeast		All Quadrants		Any
	30+	30-	30+	30-	30+	30-	30+	30-	30+	30-	
< 5	2	1	1	1	1	1	5	1	9	4	13
5 - 6	3	10	0	6	4	5	2	1	9	22	31
6 - 7	4	29	2	21	1	7	3	9	10	66	76
> 7	0	40	0	37	0	26	1	29	1	132	133
Sunlit	9	80	3	65	6	39	11	40	29	224	253
Shadow	0	0	0	0	0	32	0	40	0	72	72
All	9	80	3	65	6	71	11	80	29	296	325

Latitude 10.0, solar az. 273.3, solar el. -18.0, solar dec. 0.0

Magnitude	Northwest		Southwest		Southeast		Northeast		All Quadrants		Any
	30+	30-	30+	30-	30+	30-	30+	30-	30+	30-	
< 5	1	1	0	0	1	0	1	0	3	1	4
5 - 6	2	16	1	10	3	0	1	1	7	27	34
6 - 7	4	20	2	16	1	2	3	2	10	40	50
> 7	2	43	0	39	0	12	0	11	2	105	107
Sunlit	9	80	3	65	5	14	5	14	22	173	195
Shadow	0	0	0	0	1	57	6	66	7	123	130
All	9	80	3	65	6	71	11	80	29	296	325

Latitude 10.0, solar az. 275.8, solar el. -30.0, solar dec. 0.0

Magnitude	Northwest		Southwest		Southeast		Northeast		All Quadrants		Any
	30+	30-	30+	30-	30+	30-	30+	30-	30+	30-	
< 5	0	0	0	0	0	0	0	0	0	0	0
5 - 6	0	1	0	0	0	0	0	0	0	1	1
6 - 7	0	13	0	6	0	0	0	0	0	19	19
> 7	0	24	0	18	0	0	0	0	0	42	42
Sunlit	0	38	0	24	0	0	0	0	0	62	62
Shadow	9	42	3	41	6	71	11	80	29	234	263
All	9	80	3	65	6	71	11	80	29	296	325

Appendix C-1-γ. Latitude 10°, solar declination +23.4°

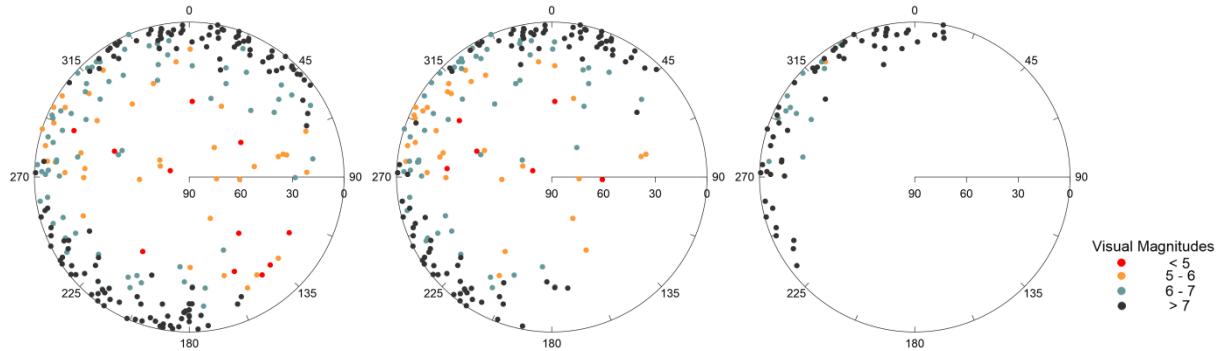


Figure C-1-γ. The distribution and brightness of Starlink satellites is illustrated for an observer at latitude +10° at the summer solstice. From left to right the Sun's distance below the western horizon is 12° (end of nautical twilight), 18° (end of astronomical twilight) and 30°.

Table C-1-γ. Latitude 10°, solar declination +23.4°

Latitude	10.0,		solar az. 296.7,		solar el. -12.0,		solar dec. 23.4		-----		
	Quadrant										
Magni-	Northwest		Southwest		Southeast		Northeast		All Quadrants		
tude	30+	30-	30+	30-	30+	30-	30+	30-	30+	30-	Any
< 5	2	1	1	0	1	4	2	0	6	5	11
5 - 6	4	15	1	2	4	4	6	3	15	24	39
6 - 7	3	33	1	15	1	4	3	10	8	62	70
> 7	0	31	0	48	0	12	0	42	0	133	133
Sunlit	9	80	3	65	6	24	11	55	29	224	253
Shadow	0	0	0	0	0	47	0	25	0	72	72
All	9	80	3	65	6	71	11	80	29	296	325

Latitude	10.0,		solar az. 298.8,		solar el. -18.0,		solar dec. 23.4		-----		
	Quadrant										
Magni-	Northwest		Southwest		Southeast		Northeast		All Quadrants		
tude	30+	30-	30+	30-	30+	30-	30+	30-	30+	30-	Any
< 5	2	2	0	0	1	0	1	0	4	2	6
5 - 6	2	19	2	2	3	0	3	1	10	22	32
6 - 7	5	30	1	11	0	1	3	6	9	48	57
> 7	0	29	0	37	0	2	0	29	0	97	97
Sunlit	9	80	3	50	4	3	7	36	23	169	192
Shadow	0	0	0	15	2	68	4	44	6	127	133
All	9	80	3	65	6	71	11	80	29	296	325

Latitude	10.0,		solar az. 304.6,		solar el. -30.0,		solar dec. 23.4		-----		
	Quadrant										
Magni-	Northwest		Southwest		Southeast		Northeast		All Quadrants		
tude	30+	30-	30+	30-	30+	30-	30+	30-	30+	30-	Any
< 5	0	0	0	0	0	0	0	0	0	0	0
5 - 6	0	1	0	0	0	0	0	0	0	1	1
6 - 7	0	12	0	0	0	0	0	0	0	12	12
> 7	0	42	0	8	0	0	0	6	0	56	56
Sunlit	0	55	0	8	0	0	0	6	0	69	69
Shadow	9	25	3	57	6	71	11	74	29	227	256
All	9	80	3	65	6	71	11	80	29	296	325

Appendix C-2- $\alpha$ . Latitude  $20^\circ$ , solar declination  $-23.4^\circ$

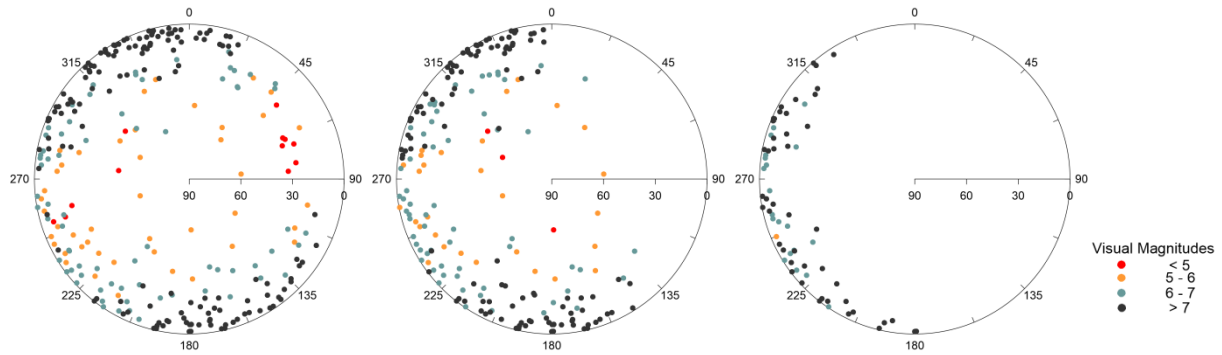


Figure C-2- $\alpha$ . The distribution and brightness of Starlink satellites is illustrated for an observer at latitude  $+20^\circ$  at the winter solstice. From left to right the Sun's distance below the western horizon is  $12^\circ$  (end of nautical twilight),  $18^\circ$  (end of astronomical twilight) and  $30^\circ$ .

Table C-2- $\alpha$ . Latitude  $20^\circ$ , solar declination  $-23.4^\circ$

Latitude 20.0, solar az. 249.2, solar el. -12.0, solar dec. -23.4											
-----											
Quadrant											
Magni-	Northwest		Southwest		Southeast		Northeast		All Quadrants		
tude	30+	30-	30+	30-	30+	30-	30+	30-	30+	30-	Any
< 5	2	0	0	3	0	0	3	4	5	7	12
5 - 6	4	5	4	16	4	3	5	3	17	27	44
6 - 7	3	18	2	27	3	9	0	9	8	63	71
> 7	0	73	0	20	0	40	0	12	0	145	145
Sunlit	9	96	6	66	7	52	8	28	30	242	272
Shadow	0	0	0	0	0	21	0	63	0	84	84
All	9	96	6	66	7	73	8	91	30	326	356

Latitude 20.0, solar az. 251.0, solar el. -18.0, solar dec. -23.4											
-----											
Quadrant											
Magni-	Northwest		Southwest		Southeast		Northeast		All Quadrants		
tude	30+	30-	30+	30-	30+	30-	30+	30-	30+	30-	Any
< 5	2	0	0	0	1	0	0	0	3	0	3
5 - 6	3	7	3	9	4	0	3	0	13	16	29
6 - 7	3	19	2	30	2	5	0	1	7	55	62
> 7	1	62	1	27	0	25	0	0	2	114	116
Sunlit	9	88	6	66	7	30	3	1	25	185	210
Shadow	0	8	0	0	0	43	5	90	5	141	146
All	9	96	6	66	7	73	8	91	30	326	356

Latitude 20.0, solar az. 253.9, solar el. -30.0, solar dec. -23.4											
-----											
Quadrant											
Magni-	Northwest		Southwest		Southeast		Northeast		All Quadrants		
tude	30+	30-	30+	30-	30+	30-	30+	30-	30+	30-	Any
< 5	0	0	0	0	0	0	0	0	0	0	0
5 - 6	0	0	0	1	0	0	0	0	0	1	1
6 - 7	0	8	0	12	0	0	0	0	0	20	20
> 7	0	19	0	25	0	2	0	0	0	46	46
Sunlit	0	27	0	38	0	2	0	0	0	67	67
Shadow	9	69	6	28	7	71	8	91	30	259	289
All	9	96	6	66	7	73	8	91	30	326	356

Appendix C-2-β. Latitude 20°, solar declination 0.0°

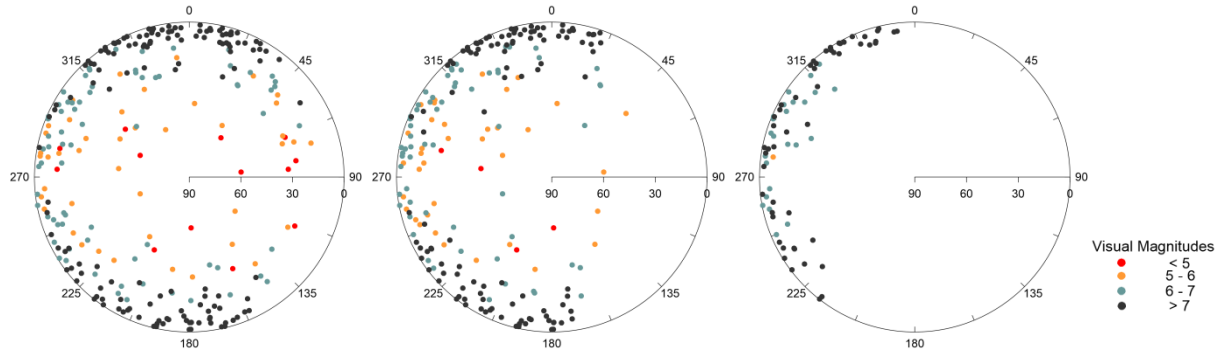


Figure C-2-β. The distribution and brightness of Starlink satellites is illustrated for an observer at latitude +20° at an equinox date. From left to right the Sun's distance below the western horizon is 12° (end of nautical twilight), 18° (end of astronomical twilight) and 30°.

Table C-2-β. Latitude 20°, solar declination 0.0°

Latitude 20.0, solar az. 274.4, solar el. -12.0, solar dec. 0.0

Magnitude	Northwest		Southwest		Southeast		Northeast		All Quadrants		Any
	30+	30-	30+	30-	30+	30-	30+	30-	30+	30-	
< 5	2	2	1	0	2	1	3	2	8	5	13
5 - 6	6	12	3	8	3	2	4	5	16	27	43
6 - 7	1	32	2	20	2	5	1	10	6	67	73
> 7	0	50	0	38	0	25	0	33	0	146	146
Sunlit	9	96	6	66	7	33	8	50	30	245	275
Shadow	0	0	0	0	0	40	0	41	0	81	81
All	9	96	6	66	7	73	8	91	30	326	356

Latitude 20.0, solar az. 276.8, solar el. -18.0, solar dec. 0.0

Magnitude	Northwest		Southwest		Southeast		Northeast		All Quadrants		Any
	30+	30-	30+	30-	30+	30-	30+	30-	30+	30-	
< 5	1	1	1	0	1	0	0	0	3	1	4
5 - 6	6	14	2	9	2	0	3	0	13	23	36
6 - 7	1	36	3	15	2	1	1	3	7	55	62
> 7	1	45	0	42	0	10	0	16	1	113	114
Sunlit	9	96	6	66	5	11	4	19	24	192	216
Shadow	0	0	0	0	2	62	4	72	6	134	140
All	9	96	6	66	7	73	8	91	30	326	356

Latitude 20.0, solar az. 282.1, solar el. -30.0, solar dec. 0.0

Magnitude	Northwest		Southwest		Southeast		Northeast		All Quadrants		Any
	30+	30-	30+	30-	30+	30-	30+	30-	30+	30-	
< 5	0	0	0	0	0	0	0	0	0	0	0
5 - 6	0	1	0	0	0	0	0	0	0	1	1
6 - 7	0	18	0	6	0	0	0	0	0	24	24
> 7	0	35	0	16	0	0	0	0	0	51	51
Sunlit	0	54	0	22	0	0	0	0	0	76	76
Shadow	9	42	6	44	7	73	8	91	30	250	280
All	9	96	6	66	7	73	8	91	30	326	356

Appendix C-2-γ. Latitude 20°, solar declination +23.4°

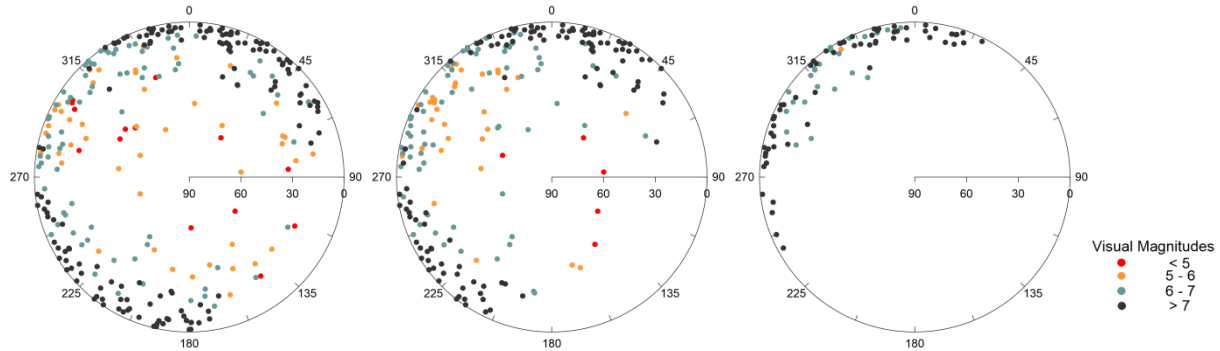


Figure C-2-γ. The distribution and brightness of Starlink satellites is illustrated for an observer at latitude +20° at the summer solstice. From left to right the Sun's distance below the western horizon is 12° (end of nautical twilight), 18° (end of astronomical twilight) and 30°.

Table C-2-γ. Latitude 20°, solar declination +23.4°

Latitude	20.0,		solar az. 300.6,		solar el. -12.0,		solar dec. 23.4		Quadrant		
Magni-	Northwest		Southwest		Southeast		Northeast		All Quadrants		Any
tude	30+	30-	30+	30-	30+	30-	30+	30-	30+	30-	
< 5	3	5	0	0	2	2	2	0	7	7	14
5 - 6	5	20	3	1	4	3	5	5	17	29	46
6 - 7	1	43	3	14	1	6	1	9	6	72	78
> 7	0	28	0	51	0	9	0	58	0	146	146
Sunlit	9	96	6	66	7	20	8	72	30	254	284
Shadow	0	0	0	0	0	53	0	19	0	72	72
All	9	96	6	66	7	73	8	91	30	326	356

Latitude	20.0,		solar az. 304.2,		solar el. -18.0,		solar dec. 23.4		Quadrant		
Magni-	Northwest		Southwest		Southeast		Northeast		All Quadrants		Any
tude	30+	30-	30+	30-	30+	30-	30+	30-	30+	30-	
< 5	1	0	0	0	2	0	2	0	5	0	5
5 - 6	5	21	0	2	2	0	1	0	8	23	31
6 - 7	3	48	4	10	0	0	3	3	10	61	71
> 7	0	27	0	39	0	0	0	46	0	112	112
Sunlit	9	96	4	51	4	0	6	49	23	196	219
Shadow	0	0	2	15	3	73	2	42	7	130	137
All	9	96	6	66	7	73	8	91	30	326	356

Latitude	20.0,		solar az. 314.3,		solar el. -30.0,		solar dec. 23.4		Quadrant		
Magni-	Northwest		Southwest		Southeast		Northeast		All Quadrants		Any
tude	30+	30-	30+	30-	30+	30-	30+	30-	30+	30-	
< 5	0	0	0	0	0	0	0	0	0	0	0
5 - 6	0	1	0	0	0	0	0	0	0	1	1
6 - 7	0	25	0	0	0	0	0	0	0	25	25
> 7	0	43	0	5	0	0	0	12	0	60	60
Sunlit	0	69	0	5	0	0	0	12	0	86	86
Shadow	9	27	6	61	7	73	8	79	30	240	270
All	9	96	6	66	7	73	8	91	30	326	356

Appendix C-3-α. Latitude 30°, solar declination -23.4°

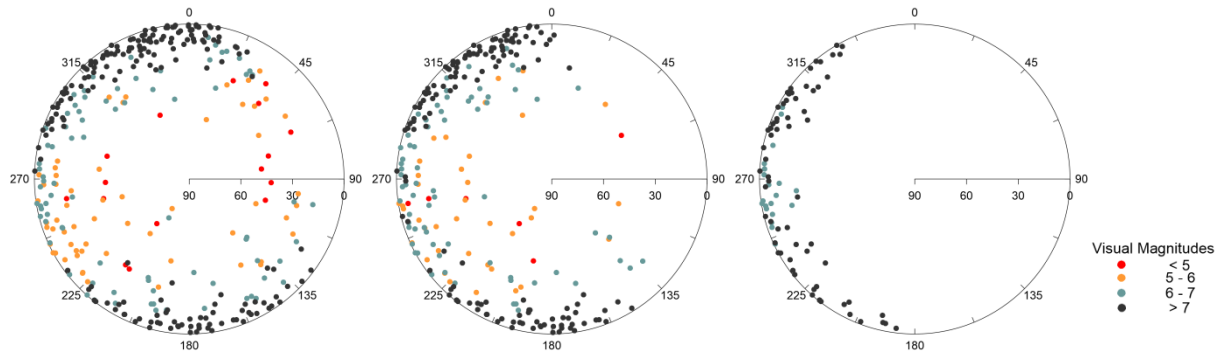


Figure C-3-α. The distribution and brightness of Starlink satellites is illustrated for an observer at latitude +30° at the winter solstice. From left to right the Sun's distance below the western horizon is 12° (end of nautical twilight), 18° (end of astronomical twilight) and 30°.

Table C-3-α. Latitude 30°, solar declination -23.4°

Latitude 30.0, solar az. 249.8, solar el. -12.0, solar dec. -23.4											
----- Quadrant -----											
Magni-	Northwest		Southwest		Southeast		Northeast		All Quadrants		
tude	30+	30-	30+	30-	30+	30-	30+	30-	30+	30-	Any
< 5	2	0	3	3	2	0	3	3	10	6	16
5 - 6	2	6	7	25	3	6	5	4	17	41	58
6 - 7	4	22	1	29	3	12	1	9	9	72	81
> 7	0	98	0	28	0	35	0	26	0	187	187
Sunlit	8	126	11	85	8	53	9	42	36	306	342
Shadow	0	0	0	0	0	29	0	88	0	117	117
All	8	126	11	85	8	82	9	130	36	423	459

Latitude 30.0, solar az. 252.9, solar el. -18.0, solar dec. -23.4											
----- Quadrant -----											
Magni-	Northwest		Southwest		Southeast		Northeast		All Quadrants		
tude	30+	30-	30+	30-	30+	30-	30+	30-	30+	30-	Any
< 5	0	0	3	2	0	0	1	0	4	2	6
5 - 6	4	6	7	18	2	0	1	0	14	24	38
6 - 7	4	26	1	30	3	4	1	0	9	60	69
> 7	0	84	0	35	0	22	0	2	0	143	143
Sunlit	8	116	11	85	5	26	3	2	27	229	256
Shadow	0	10	0	0	3	56	6	128	9	194	203
All	8	126	11	85	8	82	9	130	36	423	459

Latitude 30.0, solar az. 258.7, solar el. -30.0, solar dec. -23.4											
----- Quadrant -----											
Magni-	Northwest		Southwest		Southeast		Northeast		All Quadrants		
tude	30+	30-	30+	30-	30+	30-	30+	30-	30+	30-	Any
< 5	0	0	0	0	0	0	0	0	0	0	0
5 - 6	0	0	0	0	0	0	0	0	0	0	0
6 - 7	0	6	0	14	0	0	0	0	0	20	20
> 7	0	34	0	31	0	0	0	0	0	65	65
Sunlit	0	40	0	45	0	0	0	0	0	85	85
Shadow	8	86	11	40	8	82	9	130	36	338	374
All	8	126	11	85	8	82	9	130	36	423	459

Appendix C-3-β. Latitude 30°, solar declination 0.0°

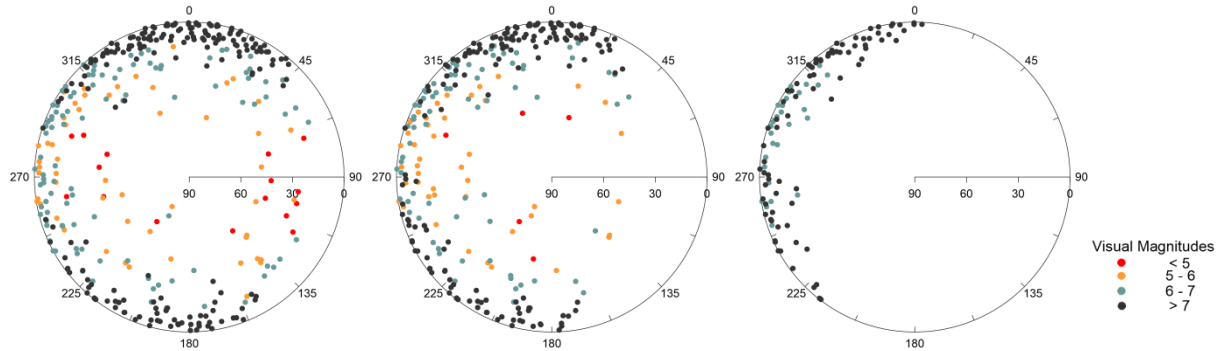


Figure C-3-β. The distribution and brightness of Starlink satellites is illustrated for an observer at latitude +30° at an equinox date. From left to right the Sun's distance below the western horizon is 12° (end of nautical twilight), 18° (end of astronomical twilight) and 30°.

Table C-3-β. Latitude 30°, solar declination 0.0°

Latitude 30.0, solar az. 277.0, solar el. -12.0, solar dec. 0.0

Magnitude	Northwest		Southwest		Southeast		Northeast		All Quadrants		Any
	30+	30-	30+	30-	30+	30-	30+	30-	30+	30-	
< 5	2	2	2	1	3	4	1	1	8	8	16
5 - 6	2	19	7	9	4	5	5	2	18	35	53
6 - 7	2	40	2	33	1	7	3	13	8	93	101
> 7	2	65	0	42	0	23	0	63	2	193	195
Sunlit	8	126	11	85	8	39	9	79	36	329	365
Shadow	0	0	0	0	0	43	0	51	0	94	94
All	8	126	11	85	8	82	9	130	36	423	459

Latitude 30.0, solar az. 280.8, solar el. -18.0, solar dec. 0.0

Magnitude	Northwest		Southwest		Southeast		Northeast		All Quadrants		Any
	30+	30-	30+	30-	30+	30-	30+	30-	30+	30-	
< 5	1	1	2	0	0	0	1	0	4	1	5
5 - 6	3	18	5	11	4	0	3	0	15	29	44
6 - 7	4	38	4	19	1	2	1	6	10	65	75
> 7	0	69	0	53	0	7	0	38	0	167	167
Sunlit	8	126	11	83	5	9	5	44	29	262	291
Shadow	0	0	0	2	3	73	4	86	7	161	168
All	8	126	11	85	8	82	9	130	36	423	459

Latitude 30.0, solar az. 289.5, solar el. -30.0, solar dec. 0.0

Magnitude	Northwest		Southwest		Southeast		Northeast		All Quadrants		Any
	30+	30-	30+	30-	30+	30-	30+	30-	30+	30-	
< 5	0	0	0	0	0	0	0	0	0	0	0
5 - 6	0	0	0	0	0	0	0	0	0	0	0
6 - 7	0	22	0	6	0	0	0	0	0	28	28
> 7	0	55	0	25	0	0	0	1	0	81	81
Sunlit	0	77	0	31	0	0	0	1	0	109	109
Shadow	8	49	11	54	8	82	9	129	36	314	350
All	8	126	11	85	8	82	9	130	36	423	459

Appendix C-3-γ. Latitude 30°, solar declination +23.4°

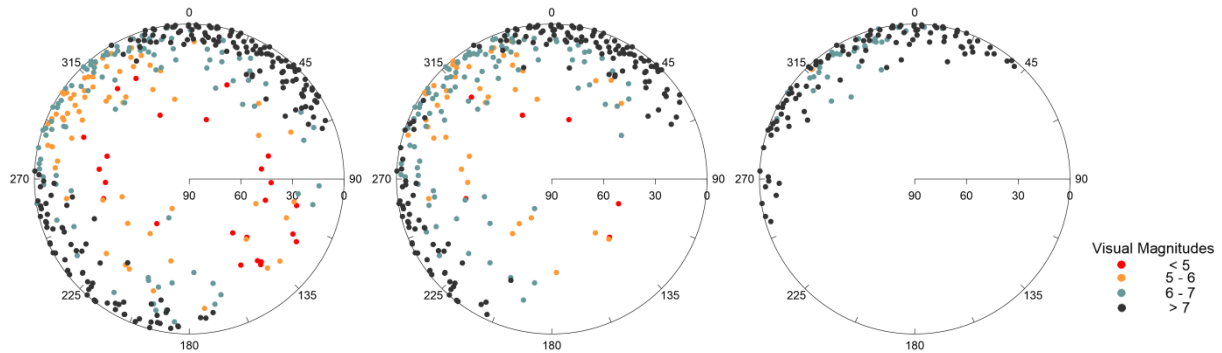


Figure C-3-γ. The distribution and brightness of Starlink satellites is illustrated for an observer at latitude +30° at the summer solstice. From left to right the Sun's distance below the western and northwestern horizon is 12° (end of nautical twilight), 18° (end of astronomical twilight) and 30°.

Table C-3-γ. Latitude 30°, solar declination +23.4°

Latitude	30.0,		solar az. 306.3,		solar el. -12.0,		solar dec. 23.4		-----		
	Quadrant										
Magni-	Northwest		Southwest		Southeast		Northeast		All Quadrants		
tude	30+	30-	30+	30-	30+	30-	30+	30-	30+	30-	Any
< 5	3	3	3	0	5	6	4	0	15	9	24
5 - 6	3	39	6	5	2	5	2	2	13	51	64
6 - 7	2	55	1	16	1	6	3	16	7	93	100
> 7	0	29	1	63	0	3	0	93	1	188	189
Sunlit	8	126	11	84	8	20	9	111	36	341	377
Shadow	0	0	0	1	0	62	0	19	0	82	82
All	8	126	11	85	8	82	9	130	36	423	459

Latitude	30.0,		solar az. 312.1,		solar el. -18.0,		solar dec. 23.4		-----		
	Quadrant										
Magni-	Northwest		Southwest		Southeast		Northeast		All Quadrants		
tude	30+	30-	30+	30-	30+	30-	30+	30-	30+	30-	Any
< 5	1	1	1	0	2	0	1	0	5	1	6
5 - 6	5	25	4	1	3	0	1	2	13	28	41
6 - 7	2	64	5	12	0	0	5	12	12	88	100
> 7	0	36	0	44	0	0	0	79	0	159	159
Sunlit	8	126	10	57	5	0	7	93	30	276	306
Shadow	0	0	1	28	3	82	2	37	6	147	153
All	8	126	11	85	8	82	9	130	36	423	459

Latitude	30.0,		solar az. 329.6,		solar el. -30.0,		solar dec. 23.4		-----		
	Quadrant										
Magni-	Northwest		Southwest		Southeast		Northeast		All Quadrants		
tude	30+	30-	30+	30-	30+	30-	30+	30-	30+	30-	Any
< 5	0	0	0	0	0	0	0	0	0	0	0
5 - 6	0	1	0	0	0	0	0	0	0	1	1
6 - 7	0	30	0	0	0	0	0	2	0	32	32
> 7	0	63	0	7	0	0	0	33	0	103	103
Sunlit	0	94	0	7	0	0	0	35	0	136	136
Shadow	8	32	11	78	8	82	9	95	36	287	323
All	8	126	11	85	8	82	9	130	36	423	459



Appendix C-4- $\alpha$ . Latitude  $40^\circ$ , solar declination  $-23.4^\circ$

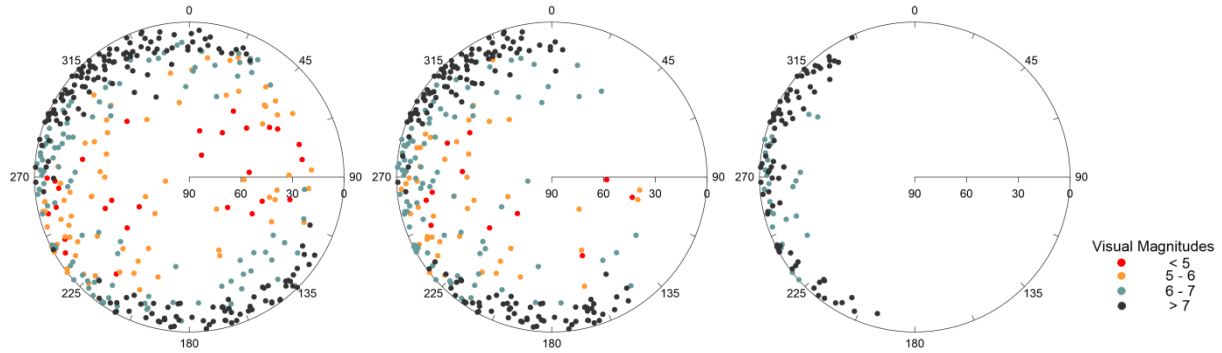


Figure C-4- $\alpha$ . The distribution and brightness of Starlink satellites is illustrated for an observer at latitude  $+40^\circ$  at the winter solstice. From left to right the Sun's distance below the western horizon is  $12^\circ$  (end of nautical twilight),  $18^\circ$  (end of astronomical twilight) and  $30^\circ$ .

Table C-4- $\alpha$ . Latitude  $40^\circ$ , solar declination  $-23.4^\circ$

Latitude 40.0, solar az. 249.4, solar el. $-12.0$ , solar dec. $-23.4$											
----- Quadrant -----											
Magni-	Northwest		Southwest		Southeast		Northeast		All Quadrants		
tude	30+	30-	30+	30-	30+	30-	30+	30-	30+	30-	Any
< 5	1	1	5	8	4	0	8	2	18	11	29
5 - 6	7	5	8	27	8	2	4	11	27	45	72
6 - 7	2	38	2	34	3	15	1	12	8	99	107
> 7	2	89	0	29	0	42	0	14	2	174	176
Sunlit	12	133	15	98	15	59	13	39	55	329	384
Shadow	0	0	0	0	0	34	0	98	0	132	132
All	12	133	15	98	15	93	13	137	55	461	516

Latitude 40.0, solar az. 254.2, solar el. $-18.0$ , solar dec. $-23.4$											
----- Quadrant -----											
Magni-	Northwest		Southwest		Southeast		Northeast		All Quadrants		
tude	30+	30-	30+	30-	30+	30-	30+	30-	30+	30-	Any
< 5	2	1	2	3	3	0	0	0	7	4	11
5 - 6	5	8	7	19	4	1	0	0	16	28	44
6 - 7	5	37	6	35	3	2	2	1	16	75	91
> 7	0	82	0	41	0	24	0	3	0	150	150
Sunlit	12	128	15	98	10	27	2	4	39	257	296
Shadow	0	5	0	0	5	66	11	133	16	204	220
All	12	133	15	98	15	93	13	137	55	461	516

Latitude 40.0, solar az. 263.4, solar el. $-30.0$ , solar dec. $-23.4$											
----- Quadrant -----											
Magni-	Northwest		Southwest		Southeast		Northeast		All Quadrants		
tude	30+	30-	30+	30-	30+	30-	30+	30-	30+	30-	Any
< 5	0	0	0	0	0	0	0	0	0	0	0
5 - 6	0	0	0	0	0	0	0	0	0	0	0
6 - 7	0	11	0	15	0	0	0	0	0	26	26
> 7	0	48	0	29	0	0	0	0	0	77	77
Sunlit	0	59	0	44	0	0	0	0	0	103	103
Shadow	12	74	15	54	15	93	13	137	55	358	413
All	12	133	15	98	15	93	13	137	55	461	516

Appendix C-4-β. Latitude 40°, solar declination 0.0°

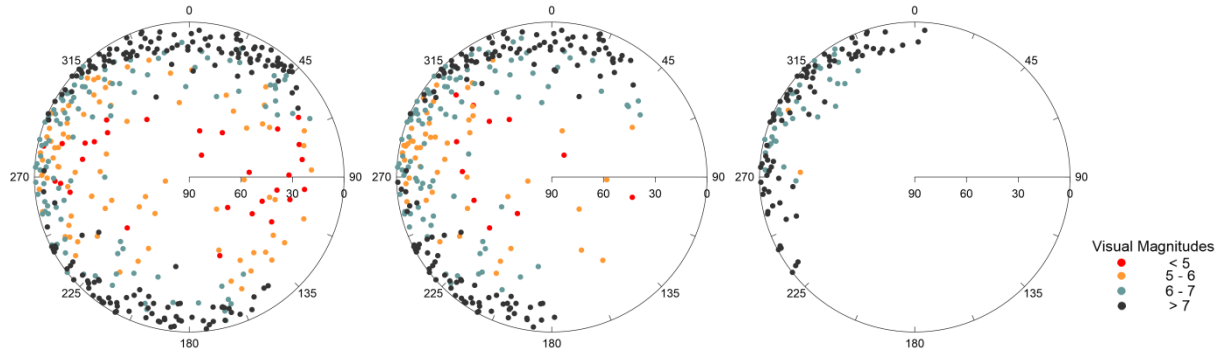


Figure C-4-β. The distribution and brightness of Starlink satellites is illustrated for an observer at latitude +40° at an equinox date. From left to right the Sun's distance below the western horizon is 12° (end of nautical twilight), 18° (end of astronomical twilight) and 30°.

Table C-4-β. Latitude 40°, solar declination 0.0°

Latitude 40.0, solar az. 280.3, solar el. -12.0, solar dec. 0.0

Magnitude	Northwest		Southwest		Southeast		Northeast		All Quadrants		
	30+	30-	30+	30-	30+	30-	30+	30-	30+	30-	Any
< 5	4	4	1	3	7	1	6	3	18	11	29
5 - 6	4	31	10	12	8	7	5	6	27	56	83
6 - 7	3	45	3	29	0	7	2	17	8	98	106
> 7	1	53	1	54	0	17	0	49	2	173	175
Sunlit	12	133	15	98	15	32	13	75	55	338	393
Shadow	0	0	0	0	0	61	0	62	0	123	123
All	12	133	15	98	15	93	13	137	55	461	516

Latitude 40.0, solar az. 285.8, solar el. -18.0, solar dec. 0.0

Magnitude	Northwest		Southwest		Southeast		Northeast		All Quadrants		
	30+	30-	30+	30-	30+	30-	30+	30-	30+	30-	Any
< 5	4	2	3	0	1	0	1	0	9	2	11
5 - 6	3	27	6	8	4	0	2	0	15	35	50
6 - 7	5	55	6	24	0	0	1	8	12	87	99
> 7	0	49	0	59	0	1	1	30	1	139	140
Sunlit	12	133	15	91	5	1	5	38	37	263	300
Shadow	0	0	0	7	10	92	8	99	18	198	216
All	12	133	15	98	15	93	13	137	55	461	516

Latitude 40.0, solar az. 299.0, solar el. -30.0, solar dec. 0.0

Magnitude	Northwest		Southwest		Southeast		Northeast		All Quadrants		
	30+	30-	30+	30-	30+	30-	30+	30-	30+	30-	Any
< 5	0	0	0	0	0	0	0	0	0	0	0
5 - 6	0	2	0	0	0	0	0	0	0	2	2
6 - 7	0	34	0	1	0	0	0	0	0	35	35
> 7	0	59	0	18	0	0	0	2	0	79	79
Sunlit	0	95	0	19	0	0	0	2	0	116	116
Shadow	12	38	15	79	15	93	13	135	55	345	400
All	12	133	15	98	15	93	13	137	55	461	516

Appendix C-4-γ. Latitude 40°, solar declination +23.4°

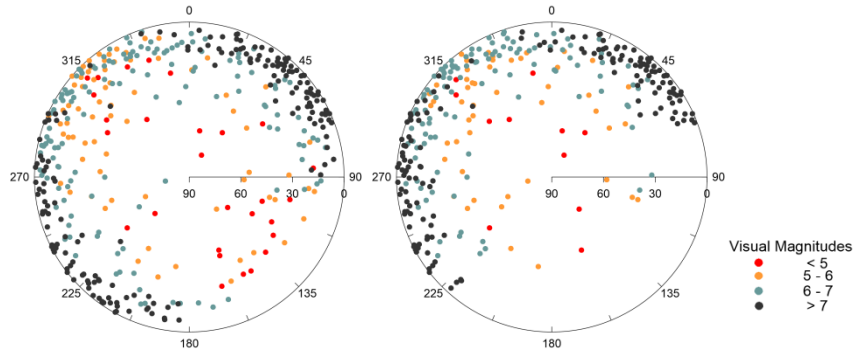


Figure C-4-γ. The distribution and brightness of Starlink satellites is illustrated for an observer at latitude +40° at the summer solstice. From left to right the Sun's distance below the northwestern horizon is 12° (end of nautical twilight) and 18° (end of astronomical twilight). The Sun does not descend to 30° below the horizon at summer solstice at this latitude.

Table C-4-γ. Latitude 40°, solar declination +23.4°

Latitude	40.0,		solar az. 315.1,		solar el. -12.0,		solar dec. 23.4		-----		
	Quadrant										
Magni-	Northwest		Southwest		Southeast		Northeast		All Quadrants		
tude	30+	30-	30+	30-	30+	30-	30+	30-	30+	30-	Any
< 5	3	6	2	0	8	4	4	1	17	11	28
5 - 6	6	36	7	3	6	5	5	4	24	48	72
6 - 7	3	70	5	22	1	6	4	28	13	126	139
> 7	0	21	1	65	0	0	0	86	1	172	173
Sunlit	12	133	15	90	15	15	13	119	55	357	412
Shadow	0	0	0	8	0	78	0	18	0	104	104
All	12	133	15	98	15	93	13	137	55	461	516

Latitude	40.0,		solar az. 324.9,		solar el. -18.0,		solar dec. 23.4		-----		
	Quadrant										
Magni-	Northwest		Southwest		Southeast		Northeast		All Quadrants		
tude	30+	30-	30+	30-	30+	30-	30+	30-	30+	30-	Any
< 5	2	3	1	0	2	0	3	0	8	3	11
5 - 6	8	22	8	0	3	0	4	4	23	26	49
6 - 7	2	69	4	11	1	0	4	18	11	98	109
> 7	0	39	0	40	0	0	0	74	0	153	153
Sunlit	12	133	13	51	6	0	11	96	42	280	322
Shadow	0	0	2	47	9	93	2	41	13	181	194
All	12	133	15	98	15	93	13	137	55	461	516

Appendix C-5- $\alpha$ . Latitude  $50^\circ$ , solar declination  $-23.4^\circ$

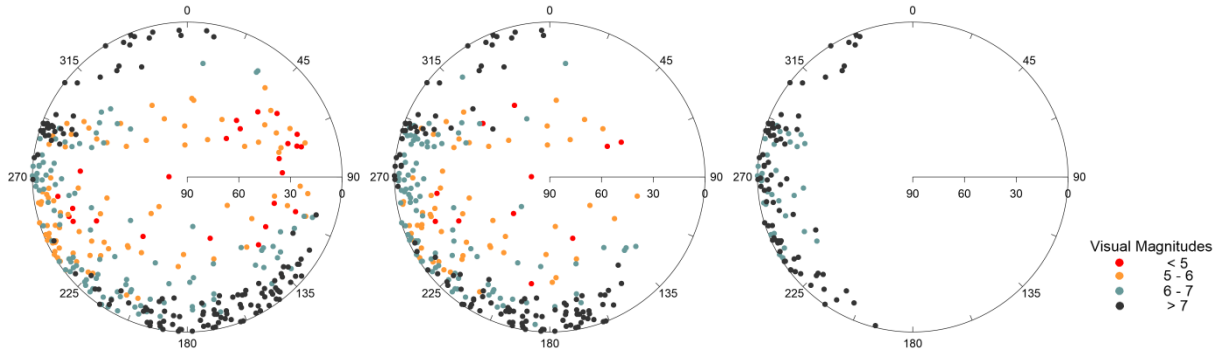


Figure C-5- $\alpha$ . The distribution and brightness of Starlink satellites is illustrated for an observer at latitude  $+50^\circ$  at the winter solstice. From left to right the Sun's distance below the western horizon is  $12^\circ$  (end of nautical twilight),  $18^\circ$  (end of astronomical twilight) and  $30^\circ$ .

Table C-5- $\alpha$ . Latitude  $50^\circ$ , solar declination  $-23.4^\circ$

Latitude 50.0, solar az. 247.8, solar el. -12.0, solar dec. -23.4											
----- Quadrant -----											
Magni-	Northwest		Southwest		Southeast		Northeast		All Quadrants		
tude	30+	30-	30+	30-	30+	30-	30+	30-	30+	30-	Any
< 5	1	1	2	4	4	1	6	5	13	11	24
5 - 6	9	7	9	41	5	4	10	4	33	56	89
6 - 7	7	17	3	56	4	20	0	3	14	96	110
> 7	0	38	0	32	0	60	0	2	0	132	132
Sunlit	17	63	14	133	13	85	16	14	60	295	355
Shadow	0	0	0	0	0	51	0	51	0	102	102
All	17	63	14	133	13	136	16	65	60	397	457

Latitude 50.0, solar az. 254.8, solar el. -18.0, solar dec. -23.4											
----- Quadrant -----											
Magni-	Northwest		Southwest		Southeast		Northeast		All Quadrants		
tude	30+	30-	30+	30-	30+	30-	30+	30-	30+	30-	Any
< 5	3	0	2	3	1	0	2	0	8	3	11
5 - 6	7	5	8	26	6	1	4	0	25	32	57
6 - 7	5	23	4	57	2	6	0	1	11	87	98
> 7	2	35	0	47	0	32	0	0	2	114	116
Sunlit	17	63	14	133	9	39	6	1	46	236	282
Shadow	0	0	0	0	4	97	10	64	14	161	175
All	17	63	14	133	13	136	16	65	60	397	457

Latitude 50.0, solar az. 268.5, solar el. -30.0, solar dec. -23.4											
----- Quadrant -----											
Magni-	Northwest		Southwest		Southeast		Northeast		All Quadrants		
tude	30+	30-	30+	30-	30+	30-	30+	30-	30+	30-	Any
< 5	0	0	0	0	0	0	0	0	0	0	0
5 - 6	0	0	0	0	0	0	0	0	0	0	0
6 - 7	0	14	0	17	0	0	0	0	0	31	31
> 7	0	34	0	42	0	0	0	0	0	76	76
Sunlit	0	48	0	59	0	0	0	0	0	107	107
Shadow	17	15	14	74	13	136	16	65	60	290	350
All	17	63	14	133	13	136	16	65	60	397	457

Appendix C-5-β. Latitude 50°, solar declination 0.0°

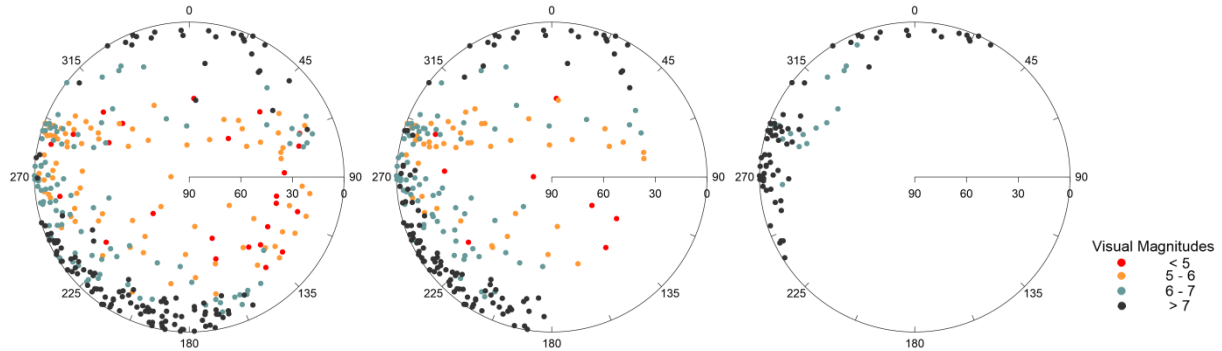


Figure C-5-β. The distribution and brightness of Starlink satellites is illustrated for an observer at latitude +40° at an equinox date. From left to right the Sun's distance below the western horizon is 12° (end of nautical twilight), 18° (end of astronomical twilight) and 30°.

Table C-5-β. Latitude 50°, solar declination 0.0°

Latitude 50.0, solar az. 284.7, solar el. -12.0, solar dec. 0.0

Magnitude	Northwest		Southwest		Southeast		Northeast		All Quadrants		
	30+	30-	30+	30-	30+	30-	30+	30-	30+	30-	Any
< 5	2	3	1	2	7	3	4	2	14	10	24
5 - 6	9	23	8	14	6	11	10	2	33	50	83
6 - 7	6	25	5	38	0	12	1	8	12	83	95
> 7	0	12	0	79	0	19	1	15	1	125	126
Sunlit	17	63	14	133	13	45	16	27	60	268	328
Shadow	0	0	0	0	0	91	0	38	0	129	129
All	17	63	14	133	13	136	16	65	60	397	457

Latitude 50.0, solar az. 292.8, solar el. -18.0, solar dec. 0.0

Magnitude	Northwest		Southwest		Southeast		Northeast		All Quadrants		
	30+	30-	30+	30-	30+	30-	30+	30-	30+	30-	Any
< 5	1	2	0	1	3	0	1	0	5	3	8
5 - 6	11	16	6	4	2	0	7	0	26	20	46
6 - 7	5	25	8	35	0	0	3	1	16	61	77
> 7	0	20	0	76	0	0	0	13	0	109	109
Sunlit	17	63	14	116	5	0	11	14	47	193	240
Shadow	0	0	0	17	8	136	5	51	13	204	217
All	17	63	14	133	13	136	16	65	60	397	457

Latitude 50.0, solar az. 313.5, solar el. -30.0, solar dec. 0.0

Magnitude	Northwest		Southwest		Southeast		Northeast		All Quadrants		
	30+	30-	30+	30-	30+	30-	30+	30-	30+	30-	Any
< 5	0	0	0	0	0	0	0	0	0	0	0
5 - 6	0	0	0	0	0	0	0	0	0	0	0
6 - 7	2	12	0	1	0	0	0	0	2	13	15
> 7	0	41	0	16	0	0	0	8	0	65	65
Sunlit	2	53	0	17	0	0	0	8	2	78	80
Shadow	15	10	14	116	13	136	16	57	58	319	377
All	17	63	14	133	13	136	16	65	60	397	457

Appendix C-5-γ. Latitude 50°, solar declination +23.4°

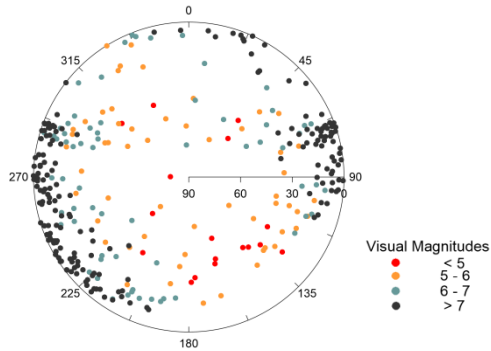


Figure C-5-γ. The distribution and brightness of Starlink satellites is illustrated for an observer at latitude +40° at the summer solstice. The Sun's distance below the northwestern horizon is 12° (end of nautical twilight). The Sun does not descend to 18° (end of astronomical twilight) or 30° below the horizon at summer solstice at this latitude.

Table C-5-γ. Latitude 50°, solar declination +23.4°

Latitude	50.0,		solar az. 332.2,		solar el. -12.0,		solar dec. 23.4		-----		
	-----										
	Quadrant										
	Northwest		Southwest		Southeast		Northeast		All Quadrants		
Magni-	30+	30-	30+	30-	30+	30-	30+	30-	30+	30-	Any
tude											
< 5	3	0	2	0	8	2	2	0	15	2	17
5 - 6	9	11	7	4	5	12	6	2	27	29	56
6 - 7	5	18	4	21	0	6	6	6	15	51	66
> 7	0	34	1	80	0	13	2	54	3	181	184
Sunlit	17	63	14	105	13	33	16	62	60	263	323
Shadow	0	0	0	28	0	103	0	3	0	134	134
All	17	63	14	133	13	136	16	65	60	397	457

Appendix C-6- $\alpha$ . Latitude  $60^\circ$ , solar declination  $-23.4^\circ$

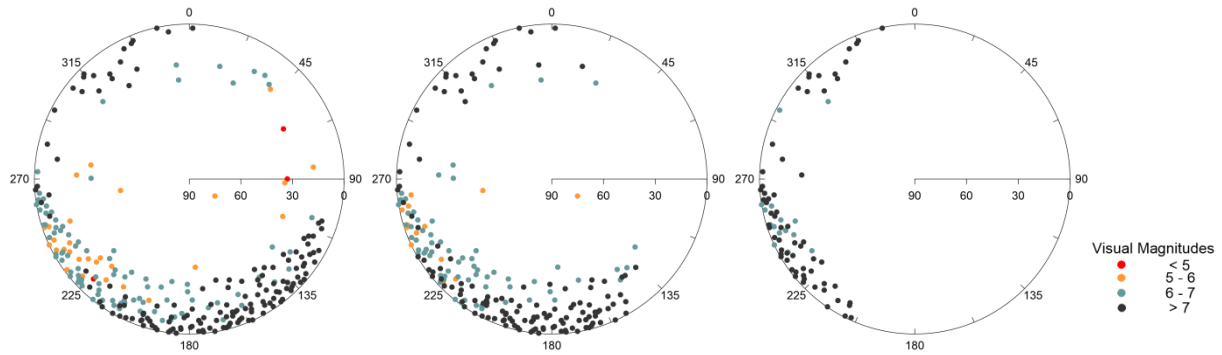


Figure C-6- $\alpha$ . The distribution and brightness of Starlink satellites is illustrated for an observer at latitude  $+60^\circ$  at the winter solstice. From left to right the Sun's distance below the western horizon is  $12^\circ$  (end of nautical twilight),  $18^\circ$  (end of astronomical twilight) and  $30^\circ$ .

Table C-6- $\alpha$ . Latitude  $60^\circ$ , solar declination  $-23.4^\circ$

Latitude 60.0, solar az. 243.6, solar el. -12.0, solar dec. -23.4											
----- Quadrant -----											
Magni-	Northwest		Southwest		Southeast		Northeast		All Quadrants		
tude	30+	30-	30+	30-	30+	30-	30+	30-	30+	30-	Any
< 5	0	0	0	1	0	0	1	1	1	2	3
5 - 6	1	1	1	19	4	0	0	2	6	22	28
6 - 7	2	3	0	70	0	12	0	5	2	90	92
> 7	0	19	0	39	0	86	0	1	0	145	145
Sunlit	3	23	1	129	4	98	1	9	9	259	268
Shadow	0	0	0	0	0	27	0	16	0	43	43
All	3	23	1	129	4	125	1	25	9	302	311

Latitude 60.0, solar az. 254.2, solar el. -18.0, solar dec. -23.4											
----- Quadrant -----											
Magni-	Northwest		Southwest		Southeast		Northeast		All Quadrants		
tude	30+	30-	30+	30-	30+	30-	30+	30-	30+	30-	Any
< 5	0	0	0	0	0	0	0	0	0	0	0
5 - 6	0	0	1	11	1	0	0	0	2	11	13
6 - 7	3	2	0	53	1	6	0	1	4	62	66
> 7	0	21	0	65	0	42	0	2	0	130	130
Sunlit	3	23	1	129	2	48	0	3	6	203	209
Shadow	0	0	0	0	2	77	1	22	3	99	102
All	3	23	1	129	4	125	1	25	9	302	311

Latitude 60.0, solar az. 274.8, solar el. -30.0, solar dec. -23.4											
----- Quadrant -----											
Magni-	Northwest		Southwest		Southeast		Northeast		All Quadrants		
tude	30+	30-	30+	30-	30+	30-	30+	30-	30+	30-	Any
< 5	0	0	0	0	0	0	0	0	0	0	0
5 - 6	0	0	0	0	0	0	0	0	0	0	0
6 - 7	0	2	0	13	0	0	0	0	0	15	15
> 7	0	17	0	45	0	0	0	0	0	62	62
Sunlit	0	19	0	58	0	0	0	0	0	77	77
Shadow	3	4	1	71	4	125	1	25	9	225	234
All	3	23	1	129	4	125	1	25	9	302	311

Appendix C-6-β. Latitude 60°, solar declination 0.0°

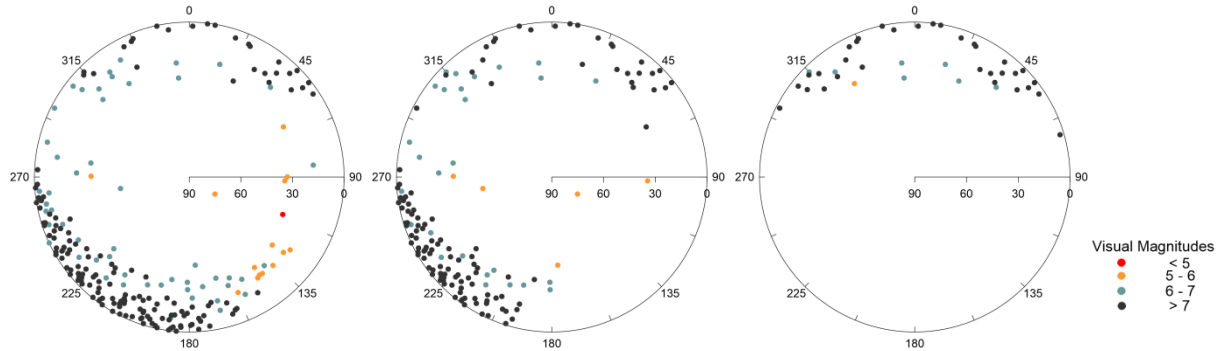


Figure C-6-β. The distribution and brightness of Starlink satellites is illustrated for an observer at latitude +40° at an equinox date. From left to right the Sun's distance below the western horizon is 12° (end of nautical twilight), 18° (end of astronomical twilight) and 30°.

Table C-6-β. Latitude 60°, solar declination 0.0°

Latitude 60.0, solar az. 291.6, solar el. -12.0, solar dec. 0.0

Magnitude	Northwest		Southwest		Southeast		Northeast		All Quadrants		Any
	30+	30-	30+	30-	30+	30-	30+	30-	30+	30-	
< 5	0	0	0	0	1	0	0	0	1	0	1
5 - 6	1	0	0	0	2	9	1	1	4	10	14
6 - 7	2	13	1	23	1	10	0	3	4	49	53
> 7	0	10	0	106	0	15	0	18	0	149	149
Sunlit	3	23	1	129	4	34	1	22	9	208	217
Shadow	0	0	0	0	0	91	0	3	0	94	94
All	3	23	1	129	4	125	1	25	9	302	311

Latitude 60.0, solar az. 304.2, solar el. -18.0, solar dec. 0.0

Magnitude	Northwest		Southwest		Southeast		Northeast		All Quadrants		Any
	30+	30-	30+	30-	30+	30-	30+	30-	30+	30-	
< 5	0	0	0	0	0	0	0	0	0	0	0
5 - 6	1	0	1	0	3	0	0	0	5	0	5
6 - 7	2	12	0	12	0	0	0	1	2	25	27
> 7	0	11	0	86	0	0	0	19	0	116	116
Sunlit	3	23	1	98	3	0	0	20	7	141	148
Shadow	0	0	0	31	1	125	1	5	2	161	163
All	3	23	1	129	4	125	1	25	9	302	311

Latitude 60.0, solar az. 0.0, solar el. -30.0, solar dec. 0.0

Magnitude	Northwest		Southwest		Southeast		Northeast		All Quadrants		Any
	30+	30-	30+	30-	30+	30-	30+	30-	30+	30-	
< 5	0	0	0	0	0	0	0	0	0	0	0
5 - 6	0	1	0	0	0	0	0	0	0	1	1
6 - 7	1	3	0	0	0	0	0	3	1	6	7
> 7	0	14	0	0	0	0	0	18	0	32	32
Sunlit	1	18	0	0	0	0	0	21	1	39	40
Shadow	2	5	1	129	4	125	1	4	8	263	271
All	3	23	1	129	4	125	1	25	9	302	311



Appendix C-6-γ. Latitude  $60^\circ$ , solar declination  $+23.4^\circ$

The Sun does not descend to  $12^\circ$  (end of nautical twilight) below the horizon at summer solstice at this latitude.

## References

- Gallozzi, S., Scardia, M., and Maris, M. 2020. Concerns about ground based astronomical observations: a step to safeguard the astronomical sky. <https://arxiv.org/pdf/2001.10952.pdf>.
- Hainaut, O.R. and Williams, A.P. 2020. Impact of satellite constellations on astronomical observations with ESO telescopes in the visible and infrared domains. *Astron. Astrophys.* manuscript no. SatConst. <https://arxiv.org/abs/2003.019pdf>.
- Halferty, G., Reddy, V., Campbell, T., Battle, A. and Furaro, R. 2022. Photometric characterization and trajectory accuracy of Starlink satellites: implications for ground-based astronomical surveys. <https://arxiv.org/abs/2208.03226>.
- Hall, J., Walker, C., Rawls, M.L., McDowell, J., Seaman, R., Venkatesan, A., Lowenthal, J., Green, R., Krafton, K. and Parriott, J. 2021. SatCon2 Working Group Reports. <https://noirlab.edu/public/media/archives/techdocs/pdf/techdoc033.pdf>.
- Hossein, S.H., Cimino, L., Rossetti, M., Gaetano, Z., Mariana, L., Curiano, F., Buccarelli, M., Seitzer, P., Santoni, F., Di Cecco, A. and Piergentili, F. 2022. Photometric characterization of Starlink satellite tracklets using RGB filters. *Adv. Space Res.*, , <https://doi.org/10.1016/j.asr.2022.07.082>.
- Krantz, H., Pearce, E.C. and Block, A. 2021. Characterizing the all-sky brightness of satellite megaconstellations and the impact on astronomy research. <https://arxiv.org/abs/2110.10578>.
- Lawler, S.M., Boley, A.C. and Rein, H. 2022. Visibility predictions for near-future satellite megaconstellations: latitudes near 50° will experience the worst light pollution. *Astron. J.*, 163, 21.
- Mallama, A. 2021. The brightness of VisorSat-design Starlink satellites. <https://arxiv.org/abs/2101.00374>.
- Mallama, 2021b. Starlink satellite brightness – characterized from 100,000 visible light magnitudes. <https://arxiv.org/abs/2111.09735>.
- Mallama, A. and Young, M. 2021. The satellite saga continues. *Sky and Telescope*, vol. 141, June, p. 16.
- Mallama, A. 2022. Newest Starlink satellites have gotten brighter again. *Sky and Telescope*, vol. 144, October, p. 10 and <https://skyandtelescope.org/astronomy-news/newest-starlink-satellites-have-gotten-brighter-again/>.
- McDowell, J. 2020. The low Earth orbit satellite population and impacts of the SpaceX Starlink constellation. *ApJ Let*, 892, L36 and <https://arxiv.org/abs/2003.07446>.

- Mroz, P., Otarola, A., Prince, T.A., Dekany, R., Duev, D.A., Graham, M.J., Groom, S.L., Masci, F.J. and Medford, M.S. 2022. Impact of the SpaceX Starlink satellites on the Zwicky Transient Facility survey observations. <https://arxiv.org/abs/2201.05343>.
- Otarola, A. (chairman) and Allen, L., Pearce, E., Krantz, H.R., Storrie-Lombardi, L., Tregloan-Reed, J., Unda-Sanzana, E., Walker, C. and Zamora, O. 2020. Draft Report of the Satellite Observations Working Group commissioned by the United Nations, Spain and the International Astronomical Union as the Workshop on Dark and Quiet Skies for Science and Society. <https://owncloud.iaa.es/index.php/s/WcdR7Z8GeqfRWxG#pdfviewer>.
- Tregloan-Reed, J., Otarola, A., Ortiz, E., Molina, V., Anais, J., Gonzalez, R., Colque, J.P. and Unda-Sanzana, E. 2020. First observations and magnitude measurement of Starlink's Darksat. *Astron. Astrophys.* 637, L1. [https://www.aanda.org/articles/aa/full\\_html/2020/05/aa37958-20/aa37958-20.html](https://www.aanda.org/articles/aa/full_html/2020/05/aa37958-20/aa37958-20.html).
- Tyson, J.A., Ivezić, Ž., Bradshaw, A., Rawls, M.L., Xin, B., Yoachim, P., Parejko, J., Greene, J., Sholl, M., Abbott, T.M.C., and Polin, D. (2020). Mitigation of LEO satellite brightness and trail effects on the Rubin Observatory LSST. arXiv e-prints, [arXiv:2006.12417](https://arxiv.org/abs/2006.12417).
- Walker, C., Hall, J., Allen, L., Green, R., Seitzer, P., Tyson, T., Bauer, A., Krafton, K., Lowenthal, J., Parriott, J., Puxley, P., Abbott, T., Bakos, G., Barentine, J., Bassa, C., Blakeslee, J., Bradshaw, A., Cooke, J., Devost, D., Galadí-Enríquez, D., Haase, F., Hainaut, O., Heathcote, S., Jah, M., Krantz, H., Kucharski, D., McDowell, J., Tregloan-Reed, J., Wainscoat, R., Williams, A., and Yoachim, P. 2020a. Impact of satellite constellations on optical astronomy and recommendations toward mitigations. *Bulletin of the Astronomical Society*, 52(2), 0206. [10.3847/25c2cfcb.346793b8](https://doi.org/10.3847/25c2cfcb.346793b8).
- Walker, C., Di Pippo, S., Aube, M., Barentine, J., Benkaldoun, Z., Benvenuti, P., Bourossis, C., Green, R., Hernshaw, J., Liszt, H., Lowenthal, J.D., Munoz-Tunon, C., Nield, K., Ricard, N., Espinosa, J.M.R., Sanhueza, P., Varela, A., Williams, A. 2020b. Dark and quiet skies for science and society. [dqskies-book-29-12-20.pdf \(iau.org\)](https://www.iau.org/public/book/29-12-20)
- Walker, C. and Benvenuti, P. (Eds.) 2022. Dark and Quiet Skies for Science and Society II. Working group reports. <https://noirlab.edu/public/media/archives/techdocs/pdf/techdoc051.pdf>.
- Williams, A., Hainaut O., Otarola A., Tan G.H., Rotola, G. 2021a. Analysing the impact of satellite constellations and ESO's role in supporting the astronomy community. <https://arxiv.org/abs/2108.04005>.

Williams, A, Hainaut O., Otarola A., Tan G.H., Biggs, A., Phillips, N. and Rotola, G. 2021b. A report to ESO Council on the impact of satellite constellations. <https://arxiv.org/abs/2108.03999>.

Witze, A. 2022. 'Unsustainable': how satellite swarms pose a rising threat to astronomy. <https://www.nature.com/articles/d41586-022-01420-9>.